CHAPTER TWO

NMR Studies on the Dynamics of Hydrogen Bonds and Ion Pairs Involving Lysine Side Chains of Proteins

Levani Zandarashvili, Alexandre Esadze, Junji Iwahara[1]
Department of Biochemistry and Molecular Biology, Sealy Center for Structural Biology and Molecular Biophysics, University of Texas Medical Branch, Galveston, Texas, USA
[1]Corresponding author: e-mail address: j.iwahara@utmb.edu

Contents

Advances in Protein Chemistry and Structural Biology, Volume 93
ISSN 1876-1623
http://dx.doi.org/10.1016/B978-0-12-416596-0.00002-6

Abstract

Hydrogen bonds and ion pairs involving side chains play vital roles in protein functions such as molecular recognition and catalysis. Despite the wealth of structural information about hydrogen bonds and ion pairs at functionally crucial sites on proteins, the dynamics of these fundamental chemical interactions are not well understood largely due to the lack of suitable experimental tools in the past. NMR spectroscopy is a powerful tool for investigations of protein dynamics, but the vast majority of NMR methods had been applicable only to the backbone or methyl groups. Recently, a substantial progress has been made in the research on the dynamics of hydrogen bonds and ion pairs involving lysine side-chain NH_3^+ groups. Together with computational/theoretical approaches, the new NMR methods provide unique insights into the dynamics of hydrogen bonds and ion pairs involving lysine side chains. Here, the methodology and its applications are reviewed.

1. INTRODUCTION

NMR spectroscopy is a versatile and powerful tool for investigations of protein dynamics. There are a wide variety of NMR methods that can provide temporal and/or spatial information on protein dynamics. NMR relaxation-based "model-free" approach has gained widespread popularity in research on protein dynamics on the ps–ns timescale (Lipari & Szabo, 1982; Palmer, 2001). Relaxation dispersion spectroscopy can yield insights into slower processes on the μs–ms timescale (Korzhnev & Kay, 2008; Loria, Berlow, & Watt, 2008; Palmer, Kroenke, & Loria, 2001). Residual dipolar coupling can provide information on protein dynamics as well (Bax, 2003; Lakomek et al., 2008; Tolman, 2001). NMR paramagnetic relaxation enhancement has also become an important tool for investigating protein dynamics (Clore & Iwahara, 2009). Quantitative studies of macromolecular processes slower than milliseconds can be carried out using techniques such as heteronuclear z-exchange spectroscopy (Farrow, Zhang, Forman-Kay, & Kay, 1994; Sahu, Clore, & Iwahara, 2007) and the fast-acquisition heteronuclear spectroscopy (Schanda & Brutscher, 2005; Schanda, Forge, & Brutscher, 2007). Although there are a large number of NMR methods for investigating the protein dynamics, most of the methods are applicable only to backbone or methyl groups.

Hydrogen bonds and ion pairs involving protein side chains are of fundamental importance in protein functions such as molecular recognition and catalysis. Owing to the advancement of structural biology, structural aspects of the hydrogen bonds and ion pairs at functionally important sites of proteins are well known. However, the dynamic properties of hydrogen bonds and ion pairs involving side chains are not well understood primarily due to the lack of suitable methodology in the past. Recently, a substantial progress has been made in the research on the dynamics of hydrogen bonds and ion pairs involving protein side chains. Integration of the new NMR spectroscopic methods with computational/theoretical approaches allowed us to gain unique insights into the dynamics of hydrogen bonds and ion pairs involving protein side chains. In this chapter, we review the new methodology and its application to lysine side chains that are important for protein functions.

2. NMR OF LYSINE SIDE-CHAIN AMINO GROUPS

2.1. $^{1}H/^{15}N$ resonances and hydrogen exchange

With a typical pKa being ~10.5 (Brown, De Marco, Wagner, & Wuthrich, 1976; Gao, DeRose, Kirby, & London, 2006; Gao et al., 2006), amino groups of lysine side chains are positively charged as NH_3^+ at neutral and acidic pH. For NMR studies of lysine side-chain NH_3^+ groups, a major challenge is their rapid hydrogen exchange with water. Hydrogen exchange rates for lysine amino groups typically exceed 1000 s^{-1} at a physiological pH and temperature, making the direct ^{1}H NMR detection of lysine NH_3^+ groups in proteins hard (Liepinsh & Otting, 1996; Segawa, Kateb, Duma, Bodenhausen, & Pelupessy, 2008). However, three factors can make the hydrogen exchange rate for a lysine side chain less than 100 s^{-1}, permitting direct ^{1}H detection: (1) structural effects (e.g., steric hindrance and hydrogen bonds) that make the hydrogen exchange slower, (2) low pH, and (3) low temperature (Esadze, Li, Wang, Brüschweiler, & Iwahara, 2011; Iwahara, Jung, & Clore, 2007; Poon et al., 2006; Takayama, Castaneda, Chimenti, Garcia-Moreno, & Iwahara, 2008; Tomlinson, Ullah, Hansen, & Williamson, 2009). In general, a reduction of pH by one unit reduces the hydrogen exchange rate by a factor of 10 (Englander, Downer, & Teitelbaum, 1972; Liepinsh & Otting, 1996). With an activation energy for the hydrogen exchange ~9 kcal mol^{-1}, hydrogen exchange for a lysine NH_3^+ group at 2 °C occurs roughly 20-fold more slowly than at 32 °C (Segawa et al., 2008).

Typical ^{15}N chemical shifts are 31–35 ppm for lysine NH_3^+ groups (e.g., see Fig. 2.1A); and 21–26 ppm for lysine NH_2 groups (Andre, Linse, & Mulder, 2007; Poon et al., 2006; Takayama et al., 2008). In a standard $^1H—^{15}N$ HSQC experiment for protein backbone amide groups with the ^{15}N carrier position ~118 ppm, the performance of ^{15}N 180° pulses and decoupling schemes is poor for NH_3 signals ~33 ppm due to the limited rf strength employed for ^{15}N (typically ~5.2 kHz for hard pulses; ~1.2 kHz for decoupling). Signals from lysine side-chain amino groups are typically unnoticeable in standard HSQC spectra for protein backbone amide groups at high magnetic field, even if the hydrogen exchange rates are slow enough to permit the observation of NH_3^+ resonances.

Use of D_2O for NMR lock in the sample buffer produces isotopic isomers of lysine amino groups (e.g., NDH_2^+ and ND_2H^+). The presence of such isomers can easily be seen in NMR spectra of lysine amino groups, because the isomers exhibit slightly different chemical shifts (e.g., see Fig. 2.1B). Because these species undergo chemical exchange between each other, the presence of isomers is undesirable particularly for ^{15}N relaxation analysis of amino groups. This problem can readily be resolved by sealing the protein solution and D_2O separately in a coaxial NMR tube (Fig. 2.3B). When temperatures lower than 4 °C (the freezing point of D_2O) are required, deuterated methanol can be sealed in the outer layer of the coaxial for NMR lock (e.g., Fig. 2.1D).

2.2. Dramatic improvement of NH_3^+ signals by removal of scalar relaxation

Iwahara et al. found that ^{15}N line shapes of HSQC and HMQC signals from NH_3^+ groups were severely broadened by scalar relaxation arising from hydrogen exchange. In HSQC, a ^{15}N coherence of an NH_3^+ group, starting from a product operator term $2N_+H_z$, experiences terms N_+, $4N_+H_zH_z$, and $8N_+H_zH_zH_z$ in the t_1 evolution period. As a result, apparent transverse relaxation rates for the t_1 period are given by (Iwahara et al., 2007; Ollerenshaw, Tugarinov, & Kay, 2003):

$$R_2^{\text{in}} = R_2^{\text{slow}} + (2/3)R_{\text{sc}} \tag{2.1}$$

$$R_2^{\text{out}} = R_2^{\text{fast}} + (3/2)R_{\text{sc}} \tag{2.2}$$

$$R_{\text{sc}} = \rho_{\text{HH}} + k_{\text{ex}}^{\text{water}} \tag{2.3}$$

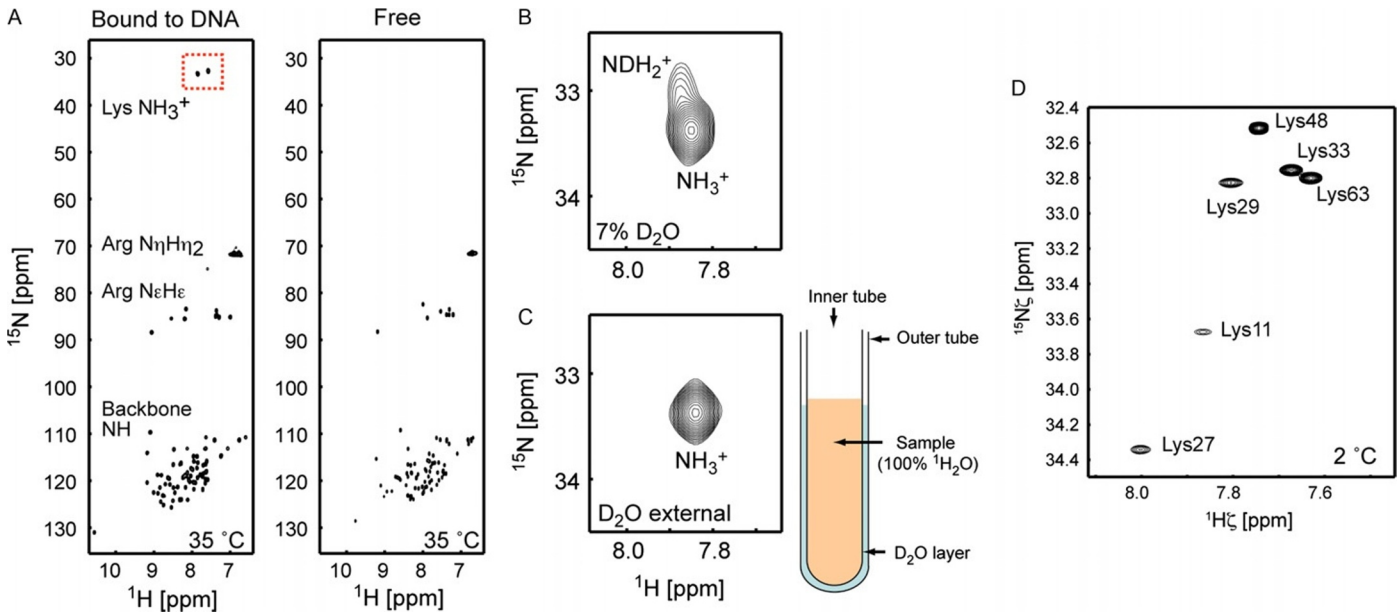

Figure 2.1 $^{1}H—^{15}N$ HSQC spectra of ^{15}N-labeled HOXD9 homeodomain. (A) 2D $^{1}H—^{15}N$ HSQC spectra measured at pH 5.8 of the protein bound specifically to a 24 bp DNA duplex (left) and in the free state (right). (B) Expansion of the F1–^{1}H-coupled HSQC spectrum showing an NH_3^+ signal at 33.3 ppm. (B and C) HSQC signals from Lys57 NH_3^+ in the $^{13}C/^{15}N$-HOXD9-DNA complex samples dissolved in (B) 93% $^{1}H_2O$ and 7% D_2O and (C) 100% $^{1}H_2O$. In (C), the NMR sample is placed in the inner tube of the coaxial system, while D_2O in the external layer between outer and inner tubes. The shoulder (the NDH_2^+) species observed in (B) is no longer present in (C). (D) HISQC spectra recorded at 2 °C for lysine NH_3^+ groups of ubiquitin in 100% $^{1}H_2O$ (pH 5) in a coaxial tube with deuterated methanol in the outer layer.

where R_2^{slow} and R_2^{fast} are the intrinsic ^{15}N relaxation rates for the inner and outer components (see Section 3.2); R_{sc}, the rate for scalar relaxation of the second kind (Abragam, 1961; Bax, Ikura, Kay, Torchi, & Tschudin, 1990) arising from one ^1H nucleus of the NH_3^+ group; ρ_{HH}, the rate for dipole–dipole (DD) interactions with external ^1H nuclei; and k_{ex}^{water}, the hydrogen exchange rate. Scalar relaxation rates for N_+, $2N_+H_z$, $4N_+H_zH_z$, and $8N_+H_zH_zH_z$ terms are given by 0, R_{sc}, $2R_{sc}$, and $3R_{sc}$, respectively. A factor of 3/2 in Eqs. (2.1) and (2.2) is due to averaging of these scalar relaxation terms. Due to a large k_{ex}^{water} for NH_3^+ groups, scalar relaxation governs the apparent transverse relaxation rates. The large effect of scalar relaxation arising from hydrogen exchange is also present in HMQC. Due to this effect, HMQC is not the best experiment for NH_3^+ groups, although both $^{13}CH_3$ and $^{15}NH_3^+$ groups are AX_3 spin systems and HMQC has been demonstrated to be optimal for CH_3 (Ollerenshaw et al., 2003; Tugarinov, Hwang, Ollerenshaw, & Kay, 2003).

To avoid the problem due to scalar relaxation arising from rapid hydrogen exchange, Iwahara et al. developed the heteronuclear in-phase single-quantum coherence (HISQC) spectroscopy (Iwahara et al., 2007). In the HISQC, the ^{15}N transverse magnetization during t_1 evolution is forced to be always in-phase (N_x or N_y) with respect to ^1H under continuous use of WALTZ-16 ^1H-decoupling rather than a single 180° pulse. Because of the absence of anti-phase terms $2N_+H_z$, $4N_+H_zH_z$, and $8N_+H_zH_zH_z$, the ^{15}N transverse relaxation during the t_1 period is completely independent of hydrogen exchange. As shown in Fig. 2.2, the ^{15}N line widths in the HISQC spectrum are strikingly narrower than in the other spectra. Although the NH_3 signal arising from Lys55 is barely discernible as a small shoulder of the Lys3 cross-peak in the HSQC and HMQC spectra recorded for the HoxD9–DNA complex, it is clearly observed as an isolated cross-peak in the HISQC spectrum. The absence of scalar relaxation in the t_1 period makes the HISQC far superior to the HSQC and HMQC. Due to scalar relaxation arising from rapid hydrogen exchange for the NH_3^+ groups, apparent transverse relaxation in the t_1 period of the HSQC or the HMQC are far faster than that of the HISQC. Indeed, the ^{15}N line shapes for the cross-peaks of the Lys3 and Lys55 NH_3^+ groups, both of which exhibit a large k_{ex}^{water} rate, are far broader in the HSQC spectrum (Fig. 2.2E) and consequently the sensitivity improvement for these cross-peaks in the HISQC spectrum (Fig. 2.2F) is even more dramatic than that for the cross-peak of Lys57 which exhibits the slowest k_{ex}^{water} rate.

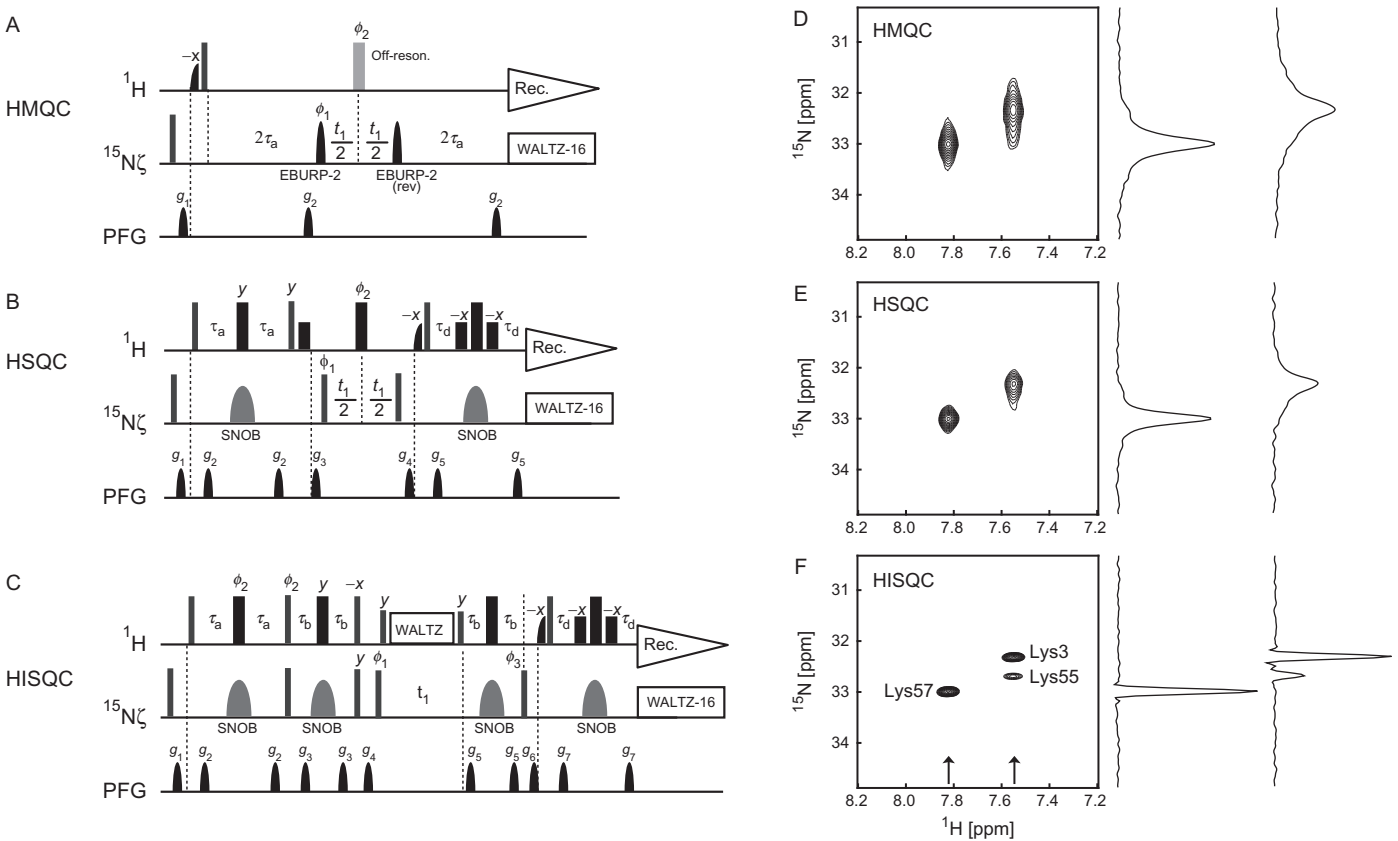

Figure 2.2 Comparison of HMQC, HSQC, and HISQC for $^{15}NH_3^+$ groups of the $^2H/^{15}N$-HOXD9 homeodomain–DNA complex (pH 5.8) at 35 °C (Iwahara et al., 2007). The pulse sequences and obtained spectra are shown for (A and D) HMQC, (B and E) HSQC, and (C and F) HISQC. For each spectrum, the ^{15}N-dimension was acquired with 140 complex points ($t_1^{max} = 168$ ms) and 8 scans per FID were accumulated, and the data were processed identically. F1 slices at the positions indicated by the arrows are shown. Contour levels and scaling of the slices are identical for all panels. *Adapted from Iwahara et al. (2007) with permission from the American Chemical Society.*

2.3. Resonance assignment of lysine NH_3^+ group

Several $^1H/^{13}C/^{15}N$ triple resonance experiments selective to lysine side chains are currently available. The selectivity to lysine side chains relies on the unique ^{15}N chemical shifts of the amino groups (see Section 2.1). By using ^{15}N pulses selective to lysine side-chain amino groups, these triple resonance experiments provide heteronuclear correlation signals only for lysine side chains. *J*-couplings relevant to lysine side-chain ^{15}N nuclei are summarized in Fig. 2.3A. Although the coherence transfer between $^{15}N\zeta—^{13}C\varepsilon$ requires a longer period due to the relatively small couplings, these experiments for NH_3^+ groups are sensitive owing to very slow relaxation of in-phase ^{15}N transverse magnetization. Figure 2.3 shows pulse sequences of the H_3NCE, H_3NCECD, $(H)CCENH_3$, HDHE(CDCE)NH, and H_2CN experiments, which are optimized for NH_3^+ groups. To avoid rapid scalar relaxation due to hydrogen exchange, it is crucially important to keep the ^{15}N transverse magnetization in-phase with respect to ^1H in these triple resonance experiments. Lysine side-chain amino $^1H/^{15}N$ resonances can be assigned by these experiments together with information on aliphatic $^1H/^{13}C$ resonances assigned with other experiments such as H(CCO)NH and C(CO)NH.

3. NMR METHODS TO INVESTIGATE INTERNAL MOTIONS OF LYSINE NH_3^+ GROUPS

3.1. Motional model and spectral density function

Here, we describe the theoretical framework as well as experimental approaches for characterization of the internal motions of lysine side-chain NH_3^+ groups. Because both $^{15}N—^1H_3$ and $^{13}C—^1H_3$ groups represent AX_3 spin systems, the theoretical framework established for ^{13}C relaxation of methyl groups in macromolecules can be directly adopted for ^{15}N relaxation of the $^{15}N—^1H_3^+$ groups owing to the following characteristics: (1) ^{15}N chemical shift anisotropy (CSA) defined as $|\sigma_{||}-\sigma_{\perp}|$ is as small as 15 ppm for lysine NH_3^+ groups (Sarkar et al., 1987), which renders CSA relaxation negligible; (2) the covalent geometry for an NH_3^+ group is almost ideally tetrahedral even in an ion pair (Lehmann, Koetzle, & Hamilton, 1971). The spin–rotation mechanism (Burke, 1970) is also negligible for the NH_3^+ groups in macromolecules at a high magnetic field (Esadze et al., 2011; Wei, Raymond, & Roberts, 1997). The DD relaxation terms and their cross-correlations govern the ^{15}N relaxation of NH_3^+ groups. For the DD autorelaxation and DD/DD cross-correlation, a general spectral

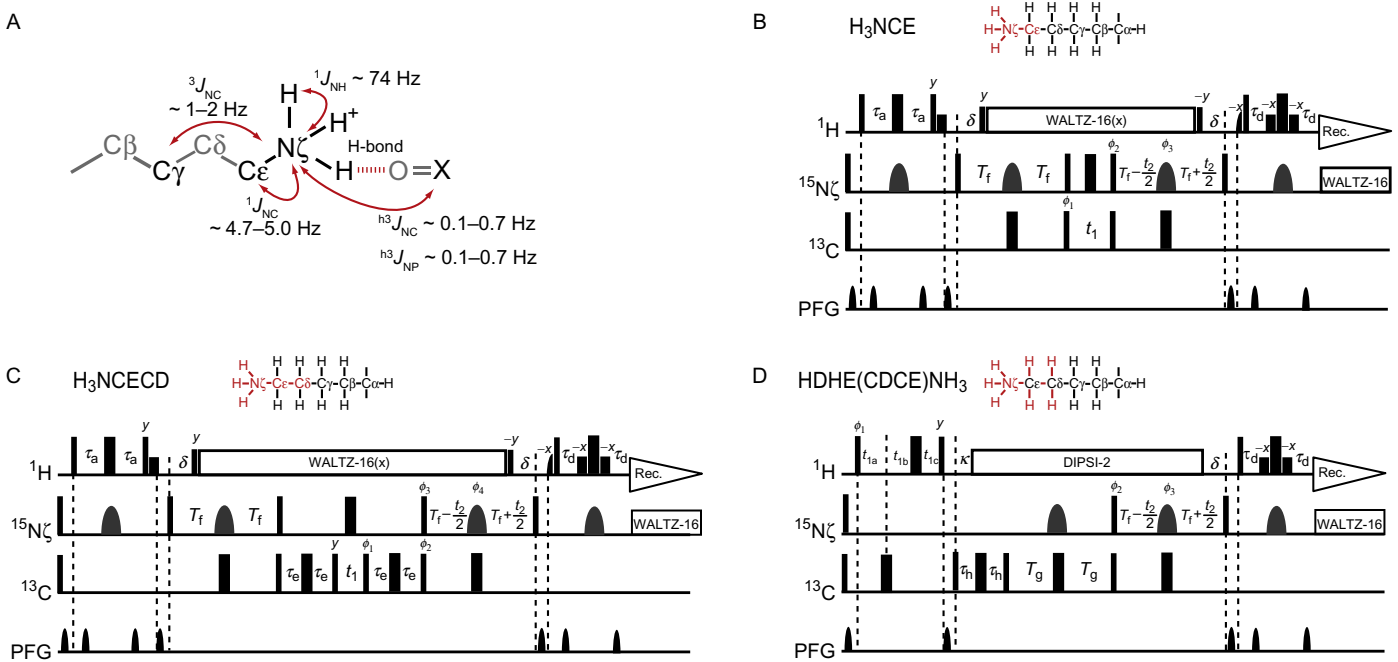

Figure 2.3 (A) Scalar ^{1}H—^{15}N and ^{13}C—^{15}N couplings for lysine side-chain amino groups (Iwahara et al., 2007; Zandarashvili, Li, Wang, Brüschweiler, & Iwahara, 2011). (B–F) 3D triple resonance experiments for the assignment of the ^{1}H and ^{15}N resonances of Lys NH_3^+ groups: (B) H_3NCE, (C) H_3NCECD, (D) $(H)CCENH_3$, (E) $HDHE(CDCE)NH_3$, and (F) H_2CN.

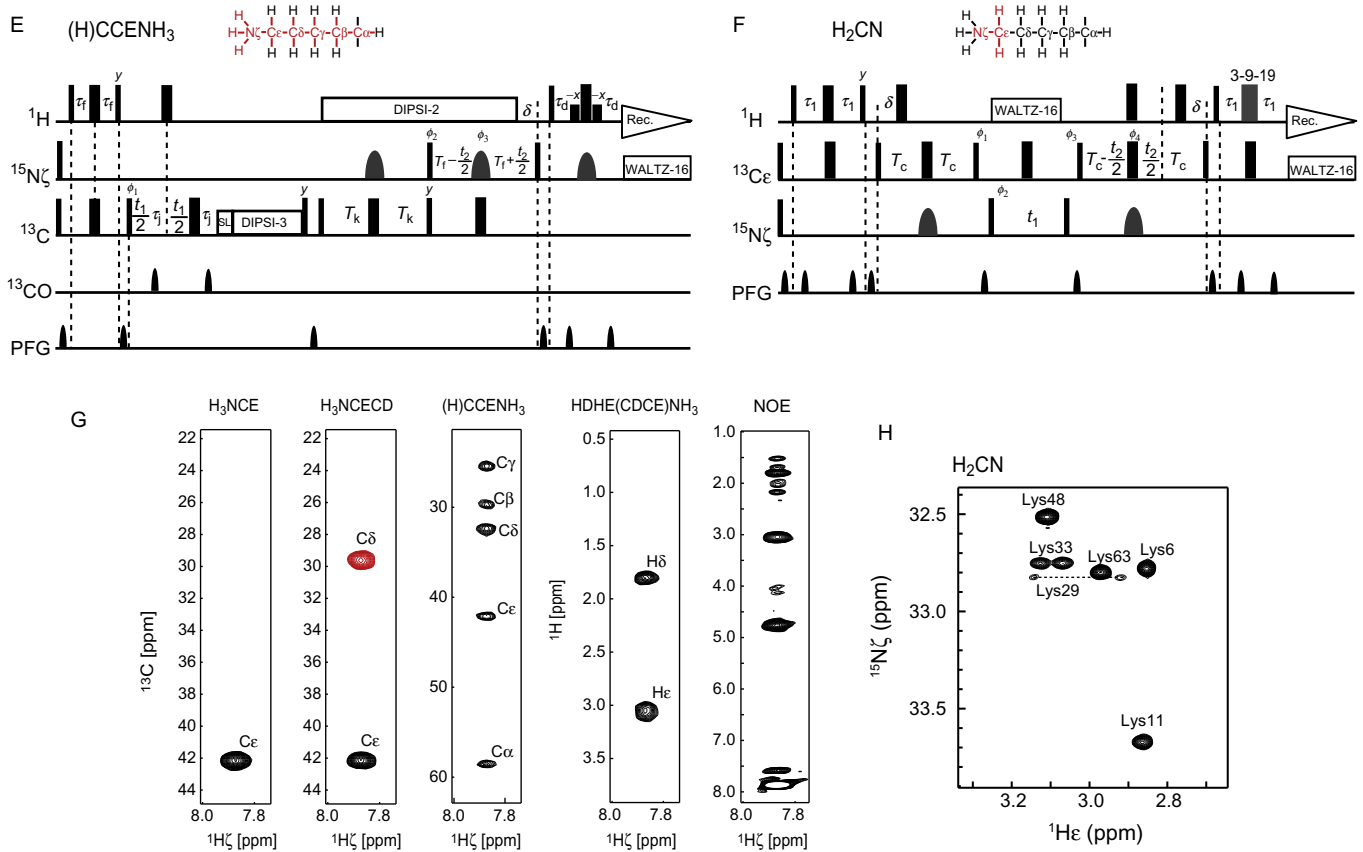

Figure 2.3—cont'd (G) 2D slices taken from the four 3D NH_3-selective triple resonance experiments illustrating correlations observed for the NH_3^+ group of Lys57 in the HoxD9–DNA complex (Iwahara et al., 2007). (H) 2D H_2(C)N spectrum recorded for ubiquitin.

density function for pairs of interacting spins ij and kl in a $^{15}N—^{1}H_3^+$ system in a macromolecule is given by (Esadze et al., 2011):

$$J_{ijkl}(\omega) = \frac{1}{4\pi}\zeta_{ij}\zeta_{kl}\left[\frac{S^2_{f,(ij,kl)}S^2_{\text{axis}}\tau_m}{1+\omega^2\tau_m^2} + \frac{S^2_{\text{axis}}\left\{P_2\left(cos\ \chi_{ij,kl}\right) - S^2_{f,(ij,kl)}\right\}\tau_1}{1+\omega^2\tau_1^2}\right.$$
$$\left. + \frac{S^2_{f,(ij,kl)}\left(1-S^2_{\text{axis}}\right)\tau_2}{1+\omega^2\tau_2^2} + \frac{\left(1-S^2_{\text{axis}}\right)\left\{P_2\left(cos\ \chi_{ij,kl}\right) - S^2_{f,(ij,kl)}\right\}\tau_3}{1+\omega^2\tau_3^2}\right] \quad (2.4)$$

where $\zeta_{ij} = \sqrt{(6\pi/5)}(\mu_0/4\pi)\gamma_i\gamma_j r_{ij}^{-3}$; μ_0, the vacuum permeability; γ, a nuclear gyromagnetic ratio; r_{ij}, the distance between spins i and j; $\chi_{ij,kl}$, the angle between the ij and kl vectors; S^2_{axis} is a generalized order parameter (Lipari & Szabo, 1982) for the symmetry axis of the AX_3 spin system; $S^2_{f,(ji,kl)}$, an order parameter for bond rotation around the symmetry axis; $P_2(x) = (3x^2-1)/2$; τ_m, the overall molecular rotational correlation time; $\tau_1^{-1} = \tau_m^{-1} + \tau_f^{-1}$; $\tau_2^{-1} = \tau_m^{-1} + \tau_i^{-1}$; $\tau_3^{-1} = \tau_m^{-1} + \tau_f^{-1} + \tau_i^{-1}$; τ_i, a correlation time for reorientation of the symmetry axis; and τ_f, a correlation time for bond rotation around the symmetry axis. The motional model for a lysine NH_3^+ group is depicted in Fig. 2.4. For autorelaxation, $i = k = N$ and

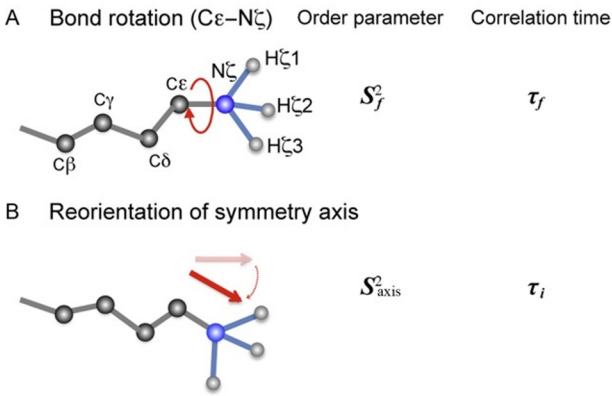

Figure 2.4 Model for internal motions of lysine NH_3^+ groups in proteins (Esadze et al., 2011). Assuming that the bond rotation (A) and reorientation of the symmetry axis (B) are not coupled, the spectral density function represented by Eq. (2.4) is derived from the product of correlation functions of overall motions, bond rotation, and reorientation of symmetry axis. Assuming ideal geometry for NH_3^+ groups (Lehmann et al., 1971), $S_f^2 = 0.111$ for $J_{\text{auto}}(\omega)$ and $J_{NHNH}(\omega)$ and $S_f^2 = 0.167$ for $J_{HHHN}(\omega)$ were used. S^2_{axis}, τ_f, and τ_i were determined from the NMR data.

$j = l = \mathrm{H}$, and the corresponding spectral density is denoted by $J_{\mathrm{auto}}(\omega)$. For N—H/N—H cross-correlation, the corresponding spectral density is denoted by $J_{NHNH}(\omega)$, for which $i = k = \mathrm{N}$, but j and l are different H spins in the spin system. Likewise, the spectral density for H—H/H—N cross-correlation is denoted by $J_{HHHN}(\omega)$, for which $i = j = \mathrm{H}$; k, another H in the AX_3 system; and $l = \mathrm{N}$. $S^2_{f,(ji,kl)}$ is given by $P_2(\cos\beta_{ij})P_2(\cos\beta_{kl})$, where β_{ij} is the angle between the vector ij and the symmetry axis. The spectral density model (Eq. 2.4) is a modification of Eq. 15 of Kay and Torchia (1991). The equations become the same if $\tau_i \gg \tau_f$. Equation 2.4 was proposed because the inequality $\tau_i \gg \tau_f$ does not necessarily hold for NH_3^+ groups, for example due to the possible presence of a hydrogen bond that may slow down the bond rotation (Esadze et al., 2011).

3.2. ^{15}N longitudinal and transverse relaxation for NH_3^+ groups

Analogous to ^{13}C longitudinal relaxation rate R_1 for CH_3 groups in proteins (Kay & Torchia, 1991), the effect of the cross-correlation between N—H DD interactions on ^{15}N R_1 of NH_3^+ groups is negligible, and ^{15}N R_1 is given by:

$$R_1 = 3J_{\mathrm{auto}}(\omega_N) + 6J_{\mathrm{auto}}(\omega_H + \omega_N) + J_{\mathrm{auto}}(\omega_H - \omega_N) \qquad (2.5)$$

Figure 2.5A shows a pulse sequence to measure ^{15}N R_1 for lysine NH_3^+ groups. In this pulse sequence as well as the other three pulse sequences in Fig. 2.5, the delay τ_b was chosen such that $3\cos^2(2\pi J_{NH}\tau_b) - 1 = 0$. In this way, the $2N_yH_z \rightarrow 4N_xH_zH_z$ transfer in the first $2\tau_b$ period and $4N_xH_zH_z \rightarrow 2N_yH_z$ in the second $2\tau_b$ period are avoided, while the $2N_yH_z \rightarrow N_x$ and $N_x \rightarrow 2N_yH_z$ transfers are retained. For CH_3 groups, the choice of the corresponding delays is known to be important for accurate ^{13}C relaxation measurements (Kay et al., 1992; Palmer, Wright, & Rance, 1991). $2N_yH_z$ and $8N_yH_zH_zH_z$ terms generated in the first $2\tau_b$ period are eliminated by a ^{1}H 90° $(-x)$ pulse and a subsequent gradient, retaining N_z during the delay T for the longitudinal relaxation measurement. The rest of the pulse sequence is the same as in the HISQC experiment.

Owing to Cε—Nζ bond rotation, ^{15}N transverse relaxation for lysine side-chain NH_3^+ groups is very slow. Due to its relatively small nuclear gyromagnetic ratio, ^{15}N transverse relaxation of an NH_3^+ group is even slower than ^{13}C transverse relaxation of a CH_3 group under the same dynamic environment. As is known for ^{13}C transverse relaxation for CH_3

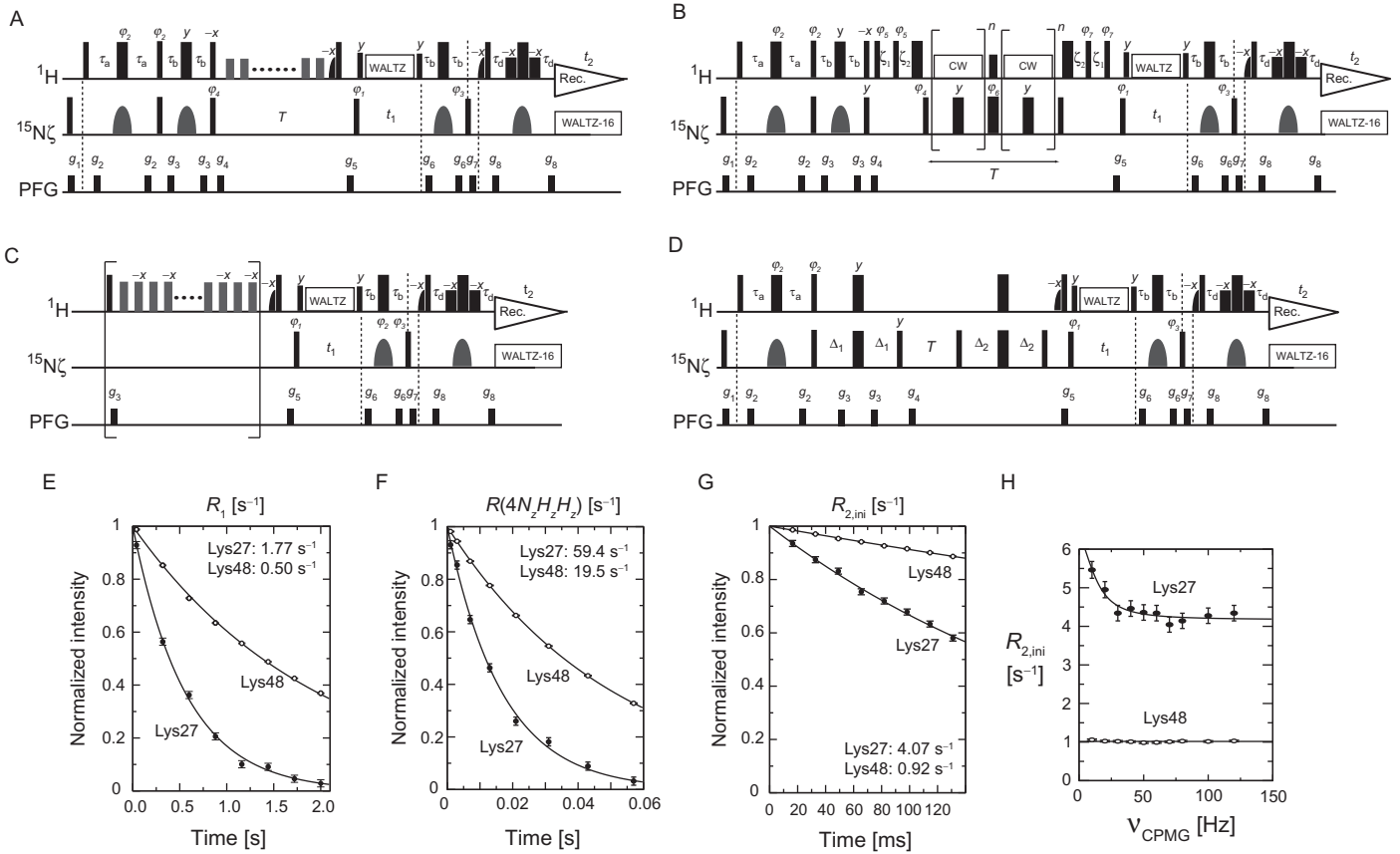

Figure 2.5 ^{15}N relaxation measurement for lysine side-chain NH_3^+ groups. (A–D) The pulse sequences for measuring ^{15}N R_1 rates (A), ^{15}N $R_{2,ini}$ rates (B), heteronuclear ^{1}H—^{15}N NOE (C), and $R(4N_zH_zH_z)$ rates (D) for NH_3^+ groups. (E–H) ^{15}N relaxation data for NH_3^+ groups of Lys27 and Lys48 of ubiquitin at 2 °C. (F) Relaxation of the longitudinal three-spin order term $4N_zH_zH_z$. (G) Transverse relaxation of the in-phase single-quantum term N_y. (H) Dependence of the initial transverse relaxation rate $R_{2,ini}$ on CPMG field strength τ_{CPMG}. *Adapted from Esadze et al. (2011) with permission from the American Chemical Society.*

groups, the ^{15}N transverse relaxation for NH_3^+ groups should be biexponential due to the strong effects of DD/DD cross-correlation between two ^{15}N—^{1}H pairs. The biexponential relaxation effects are manifested through:

$$f(T) = (3/4)\exp\left(-R_{2,\text{slow}}T\right) + (1/4)\exp\left(-R_{2,\text{fast}}T\right) \tag{2.6}$$

with the relaxation rates given by (Kay & Torchia, 1991):

$$R_{2,\text{slow}} \approx 2J_{\text{auto}}(0) - (4/3)J_{NHNH}(0) \tag{2.7}$$

$$R_{2,\text{fast}} \approx 2J_{\text{auto}}(0) + 4J_{NHNH}(0) \tag{2.8}$$

In the energy level diagram of an AX_3 spin system, the $R_{2,\text{slow}}$ rates are related to two ^{15}N transitions in the $I=3/2$ manifold and four transitions in the $I=1/2$ manifolds, whereas the $R_{2,\text{fast}}$ rates are related to two transitions in the $I=3/2$ manifold (Kay et al., 1992; Ollerenshaw et al., 2003).

Figure 2.5B shows the pulse sequence for the ^{15}N transverse relaxation measurement, in which the continuous wave (CW)-CPMG scheme (Hansen, Vallurupalli, & Kay, 2008) is implemented for maintaining the in-phase single-quantum coherence N_+ and thereby effectively eliminating the scalar relaxation during the T period. This scheme contains two CPMG blocks (Carr & Purcell, 1954; Meiboom & Gill, 1958) that sandwiches a refocusing pulse, and the ^{1}H-CW is applied during each of CPMG blocks. The application of ^{1}H-CW makes the relaxation rates for the four ^{15}N transitions associated with the $I=3/2$ manifold become equal, while the other four ^{15}N transitions in the $I=1/2$ manifolds remain unaffected (Kay et al., 1992). As a result, the overall relaxation effect during the T period is given by:

$$f(T) = (1/2)\exp\left(-R_{2,\text{ave}}T\right) + (1/2)\exp\left(-R_{2,\text{slow}}T\right) \tag{2.9}$$

for which the average ^{15}N relaxation rates $R_{2,\text{ave}}$ for the $I=3/2$ manifold are $(R_{2,\text{slow}}+R_{2,\text{fast}})/2$. The initial rate $R_{2,\text{ini}}$ for the ^{15}N transverse relaxation is given by:

$$R_{2,\text{ini}} = f'(0) = (3/4)R_{2,\text{slow}} + (1/4)R_{2,\text{fast}} \tag{2.10}$$

for both Eq. (2.6) and Eq. (2.9). As evident from Eqs. (2.7), (2.8), and (2.10), $R_{2,\text{ini}}$ is independent of the N—H/N—H cross-correlation term $J_{NHNH}(\omega)$. It is a function of $J_{\text{auto}}(\omega)$ according to (Abragam, 1961):

$$R_{2,\mathrm{ini}} = 2J_{\mathrm{auto}}(0) + (3/2)J_{\mathrm{auto}}(\omega_N) + 3J_{\mathrm{auto}}(\omega_H + \omega_N) + 3J_{\mathrm{auto}}(\omega_H) + (1/2)J_{\mathrm{auto}}(\omega_H - \omega_N) \quad (2.11)$$

Thus, the $R_{2,\mathrm{ini}}$ rates are useful for the analysis of the dynamics of the NH_3^+ groups. The biexponential decay (Eq. 2.9) and single-exponential decay according to $\exp(-R_{2,\mathrm{init}}T)$ are virtually indistinguishable for the first 30% decay, for which the use of single-exponential fitting for determination of $R_{2,\mathrm{init}}$ is valid (Esadze et al., 2011). Owing to the intrinsically slow ^{15}N transverse relaxation of NH_3^+ groups, the validity range covers the entire range of practically available ^{15}N-CPMG lengths (<150 ms). The pulse sequence shown in Fig. 2.5B can also be used to detect μs–ms timescale motions of lysine NH_3^+ groups (Esadze et al., 2011), because the CW-CPMG scheme is suitable for relaxation dispersion experiments (Baldwin, Hansen, Vallurupalli, & Kay, 2009; Hansen et al., 2008). Figure 2.5H shows examples of relaxation dispersion data for lysine NH_3^+ groups.

3.3. Heteronuclear nuclear Overhauser enhancement (NOE) and relaxation of $4N_zH_zH_z$ terms for NH_3^+ groups

Figure 2.5C shows the pulse sequence to measure heteronuclear nuclear Overhauser enhancement (NOE) for NH_3^+ groups. To achieve an ideal steady state for ^{15}N longitudinal magnetizations of NH_3^+ groups, 180° pulses instead of 120° pulses are used. When $\langle H_z \rangle$ is saturated (i.e., $\langle H_z \rangle = 0$) in the steady state, the behaviors of N_z and $4N_zH_zH_z$ terms are given by the following differential equations with cross-correlation taken into account (Kumar, Grace, & Madhu, 2000).

$$\frac{\mathrm{d}}{\mathrm{d}t}(<N_z> - N_\infty) = -R_1(<N_z> - N_\infty) + \sigma_{NH}\left(H^{\mathrm{a}}_\infty + H^{\mathrm{b}}_\infty + H^{\mathrm{c}}_\infty\right) - \Gamma_{NHNH}\left(<4N_zH^{\mathrm{a}}_zH^{\mathrm{b}}_z> + <4N_zH^{\mathrm{b}}_zH^{\mathrm{c}}_z> + <4N_zH^{\mathrm{c}}_zH^{\mathrm{a}}_z>\right) \quad (2.12)$$

$$\frac{\mathrm{d}}{\mathrm{d}t}<4N_zH_zH_z> = -R(4N_zH_zH_z)<4N_zH_zH_z> - \Gamma_{NHNH}(<N_z> - N_\infty) + \Gamma_{HHHN}H_\infty \quad (2.13)$$

where H_∞ and N_∞ represent Boltzmann magnetizations; σ_{NH}, a heteronuclear cross-relaxation rate; $R(4N_zH_zH_z)$, an autorelaxation rate for a $4N_zH_zH_z$ term; Γ_{NHNH}, N—H/N—H cross-correlation for longitudinal relaxation; and Γ_{HHHN}, H—H/H—N cross-correlation within the AX_3 spin system for longitudinal relaxation. N—H/N—H cross-correlation

inter-converts N_z and $4N_zH_zH_z$, whereas H—H/H—N cross-correlation inter-converts H_z and $4N_zH_zH_z$. The rates for cross-relaxation and cross-correlations are (Kumar et al., 2000):

$$\sigma_{NH} = 2J_{\text{auto}}(\omega_H + \omega_N) - (1/3)J_{\text{auto}}(\omega_H - \omega_N) \tag{2.14}$$

$$\Gamma_{NHNH} = 2J_{NHNH}(\omega_N) \tag{2.15}$$

$$\Gamma_{HHHN} = 2J_{HHHN}(\omega_H) \tag{2.16}$$

The pulse sequence (Fig. 2.5C) is designed so that $\langle 4N_zH_zH_z\rangle$ terms are unperturbed by ^{1}H pulses in the ^{1}H saturation period, and thereby providing a better steady state for ^{15}N longitudinal magnetization. By using ^{1}H 180° pulses instead of 120° pulses, $\langle H_z\rangle$ is saturated without perturbing $\langle 4N_zH_zH_z\rangle$ in this pulse sequence. To compensate the pulse imperfection, 180° pulses along x and $-x$ are applied alternately in the saturation period. With this pulse sequence, the heteronuclear NOE is given by:

$$\text{NOE} = 1 + 3\left(\frac{\gamma_H}{\gamma_N}\right)\frac{\sigma_{NH}R(4N_zH_zH_z) - 2\Gamma_{NHNH}\Gamma_{HHHN}}{R_1R(4N_zH_zH_z) - 3\Gamma^2_{NHNH}} \tag{2.17}$$

which is derived from Eqs. (2.12)–(2.16) with all time derivatives set to zero for the steady state. If the $R(4N_zH_zH_z)$ is much larger than the other rates involved, the heteronuclear NOE becomes:

$$\text{NOE} = 1 + 3\left(\frac{\gamma_H}{\gamma_N}\right)\frac{\sigma_{NH}}{R_1} \tag{2.18}$$

which corresponds to the standard form for the case with no cross-correlation involved.

Practically, the signal intensity for the reference spectrum in the heteronuclear NOE experiment is influenced by hydrogen exchange. If the recovery level of water magnetization is not 100%, the signal intensity for the reference spectrum can become weaker (Grzesiek & Bax, 1993; Idiyatullin, Daragan, & Mayo, 2001; Li & Montelione, 1994; Skelton et al., 1993). These effects can introduce substantial errors in the heteronuclear NOEs. In the heteronuclear NOE experiment, these problems were avoided by implementation of the water-flip-back scheme (Grzesiek & Bax, 1993) and the use of a very long recycle delay (12 s and 18 s at 600 MHz and 800 MHz, respectively). Despite the use of the very long recycle delay, measurement of the heteronuclear NOE for NH_3^+ groups can be carried out in 2–3 days owing to the slow decay during the t_1 evolution period (Anderson et al., 2013; Esadze et al., 2011).

While cross-relaxation rate σ_{NH} and cross-correlation rates Γ_{NHNH} and Γ_{HHHN} in Eq. (2.17) are a function of the correlation times and the order parameters under the assumption that the geometry of NH_3^+ groups is ideally tetrahedral, $R(4N_zH_zH_z)$ needs to be experimentally determined because it depends on other factors. The relaxation rate for $4N_zH_zH_z$ terms is given by:

$$R(4N_zH_zH_z) \approx R_1 + 2\left(\rho_{HH} + k_{ex}^{water}\right) \tag{2.19}$$

where R_1 is defined in Eq. (2.5); and ρ_{HH} is the rate of autorelaxation for a ^1H nucleus in the AX_3 system via DD interactions with external ^1H nuclei (Iwahara et al., 2007; Skrynnikov & Ernst, 1999). The hydrogen exchange rate k_{ex}^{water} typically dominates in $R(4N_zH_zH_z)$. Figure 2.5D shows the pulse sequence for the measurement of $R(4N_zH_zH_z)$ for lysine NH_3^+ groups. In this pulse sequence, $4N_zH_zH_z$ terms are created at the beginning of the delay T, and the peak intensities are measured as a function of T. Although the $4N_zH_zH_z \rightarrow N_z$ transfer via N—H/N—H cross-correlation during the delay T in this pulse sequence can contribute to the change of the intensity as a function of T, the effect can be neglected in good approximation, because Γ_{NHNH} is much smaller than $R(4N_zH_zH_z)$ for NH_3^+ groups.

3.4. Determination of order parameters and correlation times for internal motions

The measurements of ^{15}N R_1, ^{15}N $R_{2,ini}$, heteronuclear NOE, and $R(4N_zH_zH_z)$ permit the determination of the order parameter S_{axis}^2 and correlation times τ_i and τ_f of internal motions for lysine NH_3^+ groups via nonlinear least-squares fitting based on Eqs. (2.5), (2.11), (2.14)–(2.17), and (2.19). If hydrogen exchange dominates $R(4N_zH_zH_z)$, then use of only Eqs. (2.5), (2.11), and (2.18) is appropriate. For fitting, the following function that contains weighted squares for R_1, $R_{2,ini}$, and NOE is minimized:

$$\chi^2 = \sum \frac{\left(Y_{obs} - Y_{cal}\right)^2}{Y_{obs}^2} \tag{2.20}$$

where Y_{obs} and Y_{cal} stand for observed and calculated quantities, respectively, of R_1, $R_{2,ini}$, and NOE. The overall molecular rotational correlation time τ_m should be determined from the backbone ^{15}N relaxation data. The number of fitting parameters in the nonlinear least-squares fitting is three (i.e., S_{axis}^2, τ_f, and τ_i), which makes the use of relaxation data at multiple

magnetic fields desirable. Esadze et al. provided a Mathematica script for this calculation (Esadze et al., 2011).

4. NMR METHODS TO INVESTIGATE HYDROGEN-BONDING DYNAMICS OF LYSINE NH_3^+ GROUPS

4.1. Hydrogen-bond scalar coupling for lysine NH_3^+ groups

Lysine NH_3^+ groups are often involved in hydrogen bonds. The presence of the hydrogen bonds can be directly detected via NMR scalar coupling across hydrogen bonds. Hydrogen-bond scalar couplings reflect orbital overlaps in hydrogen bonds and provide unique information on hydrogen bonding (Grzesiek, Cordier, Jaravine, & Barfield, 2004). Figure 2.6 shows the NMR pulse sequences for measuring $^{15}N—^{13}C$ or $^{15}N—^{31}P$ scalar couplings ($^{h3}J_{NC}$ or $^{h3}J_{NP}$) across hydrogen bonds involving lysine NH_3^+ groups (Anderson et al., 2013; Zandarashvili et al., 2011). The pulse sequences in Fig. 2.6A and C are for two-dimensional heteronuclear correlation experiments to observe signals arising from coherence transfer via hydrogen-bond scalar couplings $^{h3}J_{NC}$ or $^{h3}J_{NP}$ for lysine NH_3^+ groups. The F_2 dimension corresponds to $^1H\zeta$ chemical shifts of the NH_3^+ groups and the F_1 dimension corresponds to ^{13}C or ^{31}P chemical shifts of nuclei coupled to $^{15}N\zeta$. Values of $|^{h3}J_{NC}|$ or $|^{h3}J_{NP}|$ can be determined using the spin-echo ^{h3}J-modulation constant-time HISQC experiments (Fig. 2.6B and D). In these experiments, which are analogous to those developed for measuring χ_1-related $^3J_{NC\gamma}$ constants (Bax et al., 1994; Hu & Bax, 1997a), two sub-spectra were recorded in an interleaved manner: one with the ^{13}C or 31P 180° pulses at positions a (sub-spectrum a), and the other at positions b (sub-spectrum b). The values of ^{h3}J constants can be calculated from $I_a / I_b = \cos 2\pi J(T_d + \delta)$, in which I_a and I_b represent signal intensities in sub-spectra a and b, respectively. Owing to very slow ^{15}N relaxation of the NH_3^+ groups, which permits the use of a long period for J-modulation, the hydrogen-bond scalar coupling constants in the range of 0.1–1.0 Hz can readily be measured for lysine NH_3^+ groups.

4.2. Estimating hydrogen-bonding lifetime from bond-rotation correlation times of NH_3^+ groups

C—N bond-rotation correlation time τ_f (see Fig. 2.4) for NH_3^+ groups can provide information on the timescale of hydrogen-bonding dynamics involving NH_3^+ groups, because the rotations of NH_3^+ groups should be

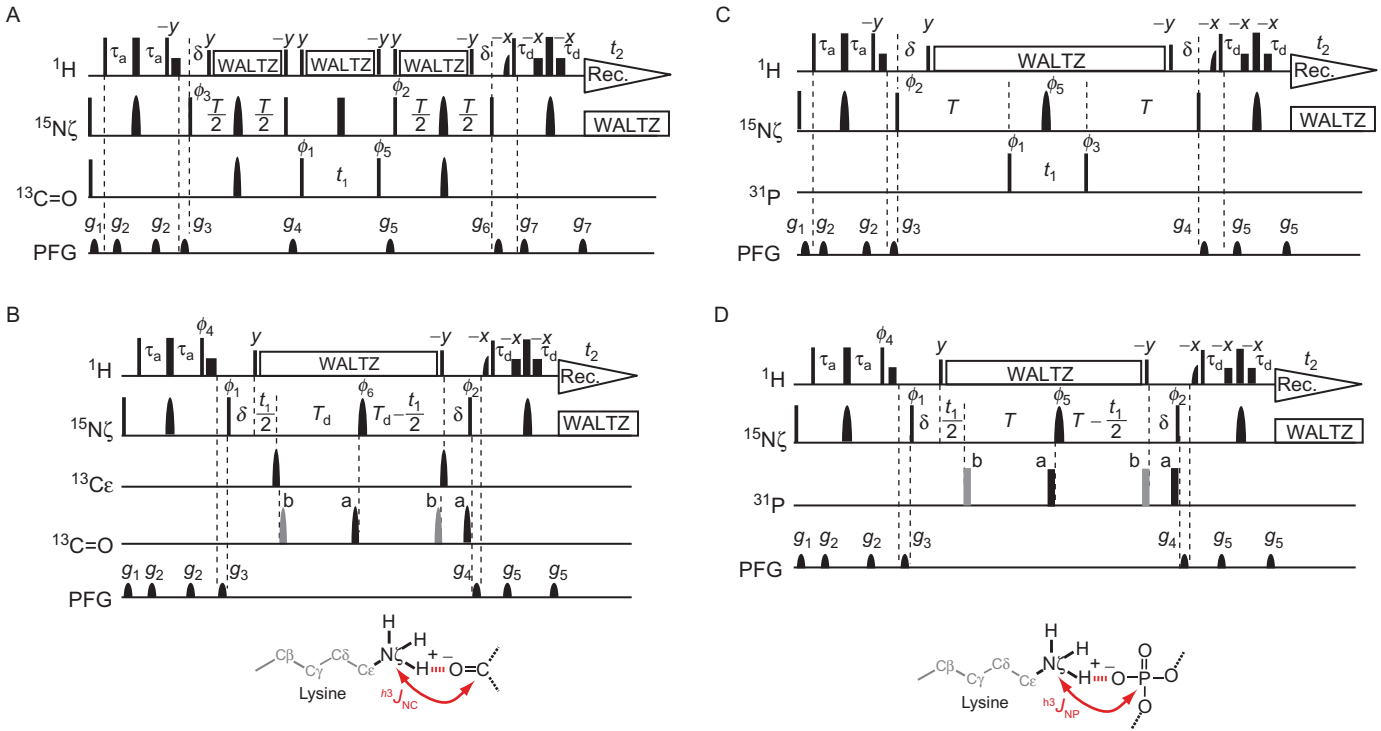

Figure 2.6 NMR pulse sequences for observing scalar couplings across hydrogen bonds involving lysine NH_3^+ groups (Anderson et al., 2013; Zandarashvili et al., 2011). (A and C) 2D heteronuclear correlation experiments for observing signals arising from coherence transfers across hydrogen bonds. Resonances of the coupling partner nuclei ($^{13}C{=}O$ for A and ^{31}P for C) are directly observed in these experiments. (B and D) 2D spin-echo *J*-modulation constant-time HISQC experiments to measure $|^{h3}J_{NC}|$ (B) or $|^{h3}J_{NP}|$ (D) coupling constants. Owing to very slow ^{15}N transverse relaxation of NH_3^+ groups, relatively long delays ($T = 212$ ms; $T_d = 206$ ms) can be used to precisely measure relatively small (0.1–0.7 Hz) hydrogen-bond scalar couplings.

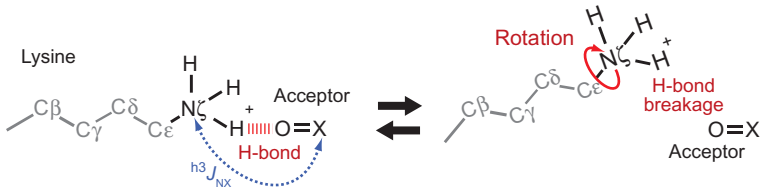

Figure 2.7 NMR-based information on hydrogen-bonding dynamics for lysine NH_3^+ groups. Hydrogen-bond scalar coupling data provide direct evidence for the hydrogen bonds. The C—N bond rotations of NH_3^+ groups should be accompanied by transient breakage of hydrogen bonds. The mean lifetime of a hydrogen bond involving an NH_3^+ group should be shorter than or comparable to the bond-rotation correlation time τ_f for the NH_3^+ group.

accompanied by transient breakage of hydrogen bonds (Esadze et al., 2011; Perrin & Gipe, 1987). The mean lifetime of a hydrogen bond involving an NH_3^+ group should be shorter than or comparable to the experimentally determined τ_f for the same NH_3^+ group (Fig. 2.7). This was confirmed by comparing the experimental bond-rotation correlation time data and the molecular dynamics (MD) data (see Section 5.3) (Esadze et al., 2011). NH_3^+ groups that do not form any hydrogen bonds typically exhibit relatively fast C—N bond rotation with τ_f around 3–25 ps, depending on temperature; NH_3^+ groups restricted by hydrogen bond(s) in a macromolecule exhibit slower (but still sub-nanosecond) bond rotations (Anderson et al., 2013; Esadze et al., 2011). However, hydrogen bonds with hydration water molecules do not seem to slow the bond rotation, presumably due to their short lifetimes (2–4 ps) (Bandyopadhyay, Chakraborty, & Bagchi, 2005). The experimental data of the bond rotation correlation time together with hydrogen-bond scalar coupling data have provided important insights into the hydrogen-bonding dynamics (Anderson et al., 2013; Esadze et al., 2011).

5. DYNAMICS OF LYSINE SIDE CHAINS OF UBIQUITIN: COMBINED USE OF NMR AND COMPUTATION

5.1. Importance of lysine side-chain NH_3^+ groups of ubiquitin

The lysine NH_3^+ groups are critically important for the function of ubiquitin, because they are linkage sites for ubiquitination involved in various cellular processes such as protein degradation (Hershko & Ciechanover, 1992), cell-cycle progression (Hershko, 1997), and immune responses

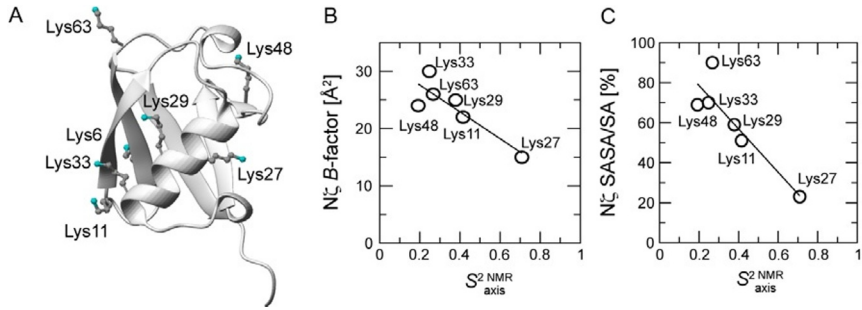

Figure 2.8 (A) Lysine side chains in the 1.8 Å resolution crystal structures of human ubiquitin (PDB code: 1UBQ). (B) Correlation between S^2_{axis} for lysine NH_3^+ groups and isotropic crystallographic *B*-factors for lysine Nζ atoms. (C) Correlation between S^2_{axis} for lysine NH_3^+ groups and solvent-accessible surface area (SASA). The vertical axis corresponds to the ratios of SASA to surface area (SA) for Nζ atoms.

(Bhoj & Chen, 2009). The ubiquitin-conjugating enzyme E2 covalently attaches ubiquitin to a target protein in the complex with the ubiquitin ligase E3. A lysine side-chain amino group of the target and the terminal carboxyl group of ubiquitin are linked in this process. The E2/E3 enzyme complex further extends the ubiquitin chain by linking a lysine side-chain NH_3^+ group of the conjugated ubiquitin to the terminal carboxyl group of the subsequent ubiquitin molecule. In this process, a polyubiquitin chain is formed and its conformation depends on the linkage site (Fushman & Walker, 2010). Human ubiquitin contains seven lysine residues: Lys6, Lys11, Lys27, Lys29, Lys33, Lys48, and Lys63 (Fig. 2.8A). The NH_3^+ group of Lys48 is the major linkage site, and the Lys48-linked polyubiquitin chain is particularly important as a marker for proteasomal degradation (Hershko & Ciechanover, 1992).

5.2. Internal motions of ubquitin's lysine NH_3^+ groups

Using ^{15}N relaxation and computation, Esadze et al. studied the internal motions of lysine side-chain NH_3^+ groups (Esadze et al., 2011). At pH 5.0 and 2 °C, the ^{15}N labeled ubiquitin exhibited six well-isolated signals from lysine amino groups in the HISQC spectrum (Fig. 2.1D). Six out of seven lysine NH_3^+ groups of ubiquitin were observed under these conditions. Lys6 was not observed in the HISQC spectrum presumably due to faster hydrogen exchange with water. In fact, a previous study reported that Lys6 side chain exhibits more than fivefold faster hydrogen exchange rates than the other lysine side chains in ubiquitin (Segawa et al., 2008). Using the

pulse sequences shown in Fig. 2.5, ^{15}N R_1, ^{15}N $R_{2,ini}$, heteronuclear $^1H—^{15}N$ NOE, and $R(4N_zH_zH_z)$ were measured for lysine NH_3^+ groups at 800 and 600 MHz ^1H frequencies. Table 2.1 shows lysine side chain ^{15}N R_1, ^{15}N $R_{2,ini}$ rates, whereas Table 2.2 shows heteronuclear $^1H—^{15}N$ NOE and $R(4N_zH_zH_z)$ parameters for lysine NH_3^+ groups. The hydrogen exchange rates k_{ex}^{water} measured at 600 MHz with CLEANEX-HISQC (Iwahara et al., 2007) are also shown in Table 2.2. Examples of the relaxation data for the NH_3^+ groups of Lys27 and Lys48 are shown in Fig. 2.5.

A remarkable aspect of ^{15}N relaxation of NH_3^+ groups is their very slow transverse relaxation, for which the initial rates $R_{2,ini}$ range from 0.98 to 4.24 s^{-1} for ubiquitin at 2 °C. The ^{15}N $R_{2,ini}$ rates of lysine NH_3^+ groups

Table 2.1 ^{15}N longitudinal and transverse relaxation rates for lysine NH_3^+ groups in human ubiquitin

	^{15}N R_1 [s^{-1}]		^{15}N $R_{2,ini}$ [s^{-1}]	
NH_3^+	800 MHz	600 MHz	800 MHz	600 MHz
Lys11	0.661 ± 0.010	0.776 ± 0.026	1.815 ± 0.089	1.629 ± 0.167
Lys27	1.431 ± 0.018	1.773 ± 0.035	4.237 ± 0.072	4.065 ± 0.132
Lys29	0.811 ± 0.003	0.933 ± 0.011	1.684 ± 0.034	1.852 ± 0.082
Lys33	0.419 ± 0.001	0.458 ± 0.002	0.971 ± 0.012	1.105 ± 0.024
Lys48	0.471 ± 0.001	0.504 ± 0.002	0.980 ± 0.010	0.915 ± 0.021
Lys63	0.404 ± 0.001	0.458 ± 0.003	1.130 ± 0.013	1.066 ± 0.026

Adapted from Esadze et al. (2011) with permission from the American Chemical Society.

Table 2.2 Heteronuclear (^1H-) ^{15}N NOE, $R(4N_zH_zH_z)$ rates, and hydrogen exchange rates k_{ex}^{water} for lysine NH_3^+ groups in human ubiquitin

	NOE		$R(4N_zH_zH_z)$ [s^{-1}]		
NH_3^+	800 MHz	600 MHz	800 MHz	600 MHz	k_{ex}^{water} [s^{-1}]
Lys11	−2.72 ± 0.09	−2.92 ± 0.17	147.1 ± 6.5	153.7 ± 17.3	71.0 ± 6.0
Lys27	−1.88 ± 0.05	−2.38 ± 0.13	59.2 ± 0.7	59.4 ± 1.4	18.7 ± 1.6
Lys29	−2.88 ± 0.05	−3.01 ± 0.09	103.1 ± 1.1	109.8 ± 2.8	43.1 ± 1.5
Lys33	−3.24 ± 0.03	−3.18 ± 0.04	42.5 ± 0.2	44.0 ± 0.2	17.6 ± 0.1
Lys48	−3.29 ± 0.02	−3.54 ± 0.03	18.1 ± 0.1	19.5 ± 0.1	8.8 ± 0.1
Lys63	−3.14 ± 0.02	−3.30 ± 0.04	40.8 ± 0.2	42.7 ± 0.2	17.1 ± 0.2

Adapted from Esadze et al. (2011) with permission from the American Chemical Society.

are 6–12-fold slower than backbone ^{15}N R_2 of the same residues. The slow $R_{2,ini}$ rates are responsible for very sharp ^{15}N line shapes of HISQC signals as shown in Fig. 2.1D. $R_{2,ini}$ rates were measured using different CPMG field strengths ν_{CPMG} for investigating the slow dynamics of the lysine side chains. The $R_{2,ini}$ rate for the NH_3^+ groups of Lys27 was found to be faster when ν_{CPMG} is small (Fig. 2.5H), while $R_{2,ini}$ rates were virtually independent of ν_{CPMG} for all the other lysine NH_3^+ groups. Provided that the slow dynamics observed for Lys27 NH_3^+ is a two-state exchange, the exchange rate for the process was calculated to be $93 \pm 33\ s^{-1}$ using expressions given by Loria, Rance, and Palmer (1999).

The ^{15}N R_1 rates for NH_3^+ groups were found to be between 0.4 and 1.8 s^{-1}. Field dependence of the ^{15}N R_1 rates was stronger than that for $R_{2,ini}$; the ^{15}N R_1 rates at 800 MHz were 10–20% smaller than those at 600 MHz. Compared to the backbone ^{15}N R_1 rates for the same lysine residues (0.89–0.94 s^{-1} at 800 MHz), the ^{15}N R_1 rates for NH_3^+ groups display larger variation. The slowest NH_3^+ R_1 rate (Lys63) was only approximately twofold slower than backbone ^{15}N R_1 of the same lysine residues.

As shown in Table 2.2, all values of the heteronuclear NOE measured for lysine NH_3^+ groups were negative and ranged from −3.54 to −1.88. $R(4N_zH_zH_z)$ rates were found to be ~40–200-fold larger than R_1 for N_z and slightly larger than two times k_{ex}^{water} (Table 2.2). This indicates that the hydrogen exchange contribution dominates in Eq. (2.19). With the observed range of $R(4N_zH_zH_z)$ rates for lysine NH_3^+ groups, where relaxation of $4N_zH_zH_z$ is dominant due to residual hydrogen exchange with water, Eq. (2.17) can be reduced to Eq. (2.18). Such approximation introduces only <3% error in heteronuclear NOE for the case of ubiquitin.

Using the experimental ^{15}N relaxation data and the spectral density model represented by Eq. (2.4), the order parameters S_{axis}^2 and correlation times τ_f and τ_i for the internal motions of NH_3^+ groups were determined. No exchange contributions to $R_{2,ini}$ were considered in the fitting procedure, because the CPMG relaxation dispersion data and the dependence of $R_{2,ini}$ on the magnetic field strength indicated the absence of exchange contributions to the $R_{2,ini}$ rates. The calculation results are shown in Table 2.3.

The order parameters S_{axis}^2 extracted for the lysine NH_3^+ groups in ubiquitin range from 0.192 to 0.709. The NH_3^+ groups of Lys11, Lys27, and Lys29, which form hydrogen bond(s) with other residues in the 1.8 Å resolution crystal structure, exhibit relatively large S_{axis}^2 values (0.415, 0.709, and 0.378, respectively), suggesting that the hydrogen bonds

Table 2.3 Order parameters S^2_{axis} and correlation times τ_f and τ_i for lysine NH_3^+ groups in human ubiquitin

NH_3^+	S^2_{axis} [a]	τ_f [ps] [b]	τ_i [ps] [c]
Lys11	0.415 ± 0.039	38 ± 71	372 ± 207
Lys27	0.709 ± 0.021	341 ± 11	0 ± 8
Lys29	0.378 ± 0.017	199 ± 24	13 ± 66
Lys33	0.248 ± 0.005	24 ± 1	114 ± 11
Lys48	0.192 ± 0.005	29 ± 1	128 ± 8
Lys63	0.267 ± 0.006	25 ± 1	100 ± 11

[a]Order parameters for the symmetry axes.
[b]Correlation times for bond rotations.
[c]Correlation times for the internal reorientational motions of the symmetry axes.
Adapted from Esadze et al. (2011) with permission from the American Chemical Society.

restrict internal motions of NH_3^+ groups. In fact, the Lys27 side chain that forms two hydrogen bonds has an order parameter larger than those of lysine side chains that display a single hydrogen bond in the crystal structure.

Interestingly, the NMR data indicate that the NH_3^+ group of Lys48, the major linkage site in ubiquitination for proteasomal degradation (Hershko & Ciechanover, 1992), is the most mobile amino group with an order parameter of 0.19. The NH_3^+ group of Lys63 is the second most abundant linkage site (Peng et al., 2003). This NH_3^+ group is also highly mobile with an order parameter of 0.27. A recent proteomic study showed that the sequence biases and structural preferences around ubiquitination sites on target proteins are similar to those of intrinsically disordered protein regions (Radivojac et al., 2010), which implicates that the lysine amino groups of the target proteins for the initial ubiquitination exhibit also a high degree of mobility. This property of the substrate lysine NH_3^+ group might be a key determinant for the efficiency of ubiquitination by the E2/E3 enzyme complex.

Figure 2.8B shows a correlation between S^2_{axis} values for the NH_3^+ groups and isotropic crystallographic *B*-factors for corresponding Nζ atoms. Although the dynamic processes that determine crystallographic *B*-factors and NMR order parameters can differ (Brüschweiler & Wright, 1994), a relatively strong anticorrelation with a correlation coefficient of −0.87 was observed between the two. Remarkably, a similar degree of correlation (correlation coefficient, −0.90) was found between the solvent-accessible surface areas of Nζ atoms and the S^2_{axis} data for the NH_3^+ groups

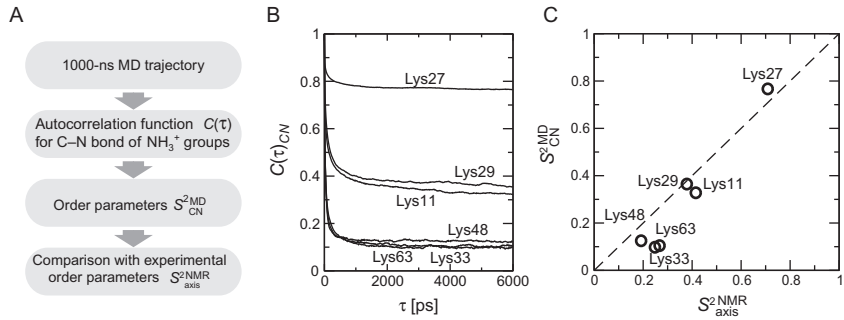

Figure 2.9 Comparison of NMR-derived experimental order parameters and MD-derived computational order parameters for lysine side-chain NH_3^+ groups of ubiquitin (Esadze et al., 2011). (A) Scheme for the comparison. (B) Autocorrelation functions for lysine Cε—Nζ bond vectors calculated from the 1000 ns MD simulation. (C) Comparison of the experimental and computational order parameters S^2_{axis} for lysine NH_3^+ groups. The horizontal axis corresponds to the S^2_{axis} extracted from experimental NMR relaxation data on the lysine NH_3^+ groups, whereas the vertical axis corresponds to the order parameters calculated as the average between 4 and 6 ns of the autocorrelation functions for the Cε—Nζ bonds obtained from the molecular dynamics simulation.

(Fig. 2.8C), which implies that interactions with water pose a major effect on the mobility of the NH_3^+ groups.

Experimental order parameters were compared with those calculated from a 1 μs MD simulation for human ubiquitin. Figure 2.9 shows the autocorrelation function from the MD trajectory and the correlation between the experimental and computational order parameters for lysine side-chain NH_3^+ groups. A reasonable agreement with a root-mean-square difference (rmsd) of 0.075 was found between them.

Dynamics of lysine side chains were investigated with NMR scalar coupling data as well (Zandarashvili et al., 2011). They measured $^3J_{N\zeta C\gamma}$ couplings between $^{15}N\zeta$ and $^{13}C\gamma$ nuclei, which are relevant to the torsion angles χ_4 of lysine side chains (Fig. 2.10). By means of Karplus equations (Cavanagh, Fairbrother, Palmer, Rance, & Skelton, 2007; Karplus, 1959), $^3J_{N\zeta C\gamma}$ coupling constants were back-calculated first from the χ_4 angles in the 1.8 Å resolution X-ray crystal structure of ubiquitin (PDB 1UBQ) (Vijay-Kumar, Bugg, & Cook, 1987). A bimodal distribution ~2 and ~0.5 Hz is found for the calculated $^3J_{N\zeta C\gamma}$ coupling constants (Fig. 2.10B), because the lysine χ_4 angles in the crystal structure are either trans or gauche. By contrast, the experimental $^3J_{N\zeta C\gamma}$ data do not exhibit such a bimodal distribution, and the agreement between the observed and calculated $^3J_{N\zeta C\gamma}$ data is poor with an rmsd of 0.91 Hz (Fig. 2.10B).

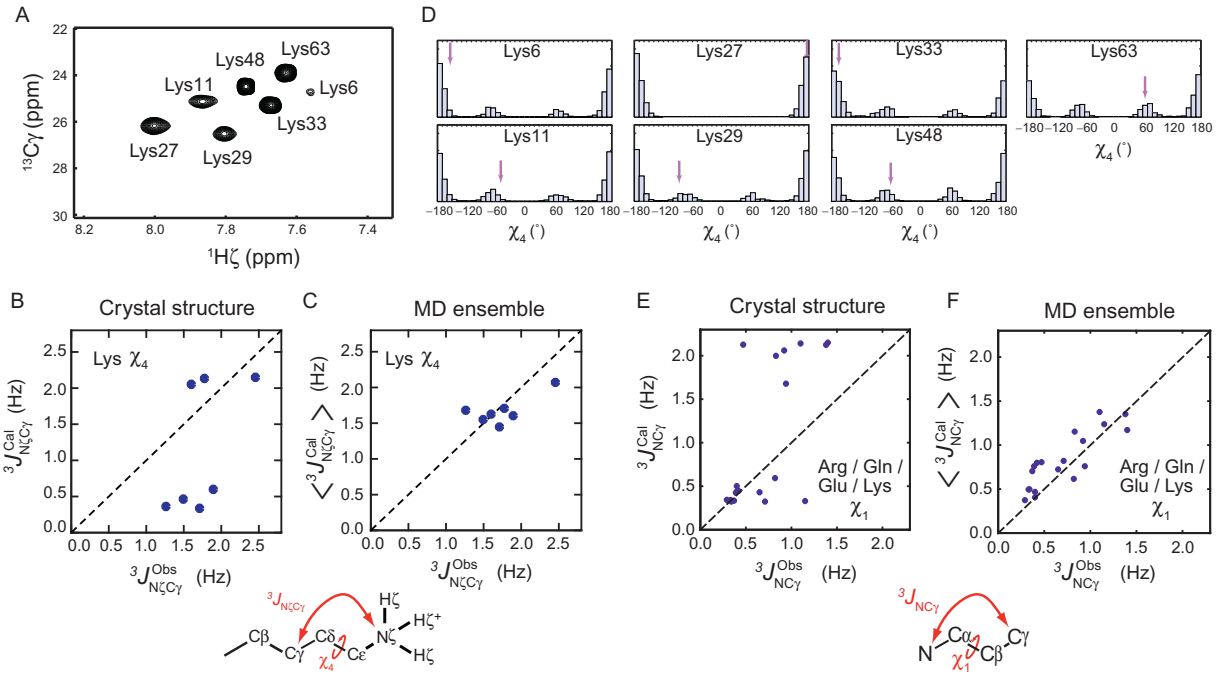

Figure 2.10 Scalar coupling data indicating side-chain torsion-angle dynamics. (A) Long-range correlation spectra recorded for lysine side-chain NH_3^+ groups in uniformly $^{13}C/^{15}N$-labeled ubiquitin. (B) Correlation between observed $^3J_{N\zeta C\gamma}$ constants and those calculated from the crystal structure (PDB 1UBQ). (C) Correlation between observed $^3J_{N\zeta C\gamma}$ constants and those calculated as ensemble averages for 1000 structures sampled every 1 ns from the 1 μs MD trajectory. (D) Histograms for the χ_4 torsion angles of individual lysine side chains of the MD ensemble. Arrows indicate the χ_4 torsion angles in the crystal structure. (E and F) Correlation between the experimental $^3J_{NC\gamma}$ data for arginine, lysine, glutamate, and glutamine residues (Hu & Bax, 1997b) and those calculated from a single crystal structure (E) or the MD ensemble (F). *Adapted from Zandarashvili et al. (2011) with permission from the American Chemical Society.*

To examine the impact of dynamics on the coupling constants, the ensemble averages $\langle {}^{3}J_{N\zeta C\gamma}\rangle$ were calculated from the χ_4 angles sampled from the 1 μs MD trajectory. Values of $\langle {}^{3}J_{N\zeta C\gamma}\rangle$ were calculated from 1000 MD snapshots sampled every 1 ns. As shown in Fig. 2.10C, $\langle {}^{3}J_{N\zeta C\gamma}\rangle$ data from the MD ensemble exhibit substantially improved agreement with the experimental ${}^{3}J_{N\zeta C\gamma}$ data (rmsd, 0.26 Hz). They also examined the impact of the dynamics on the χ_1-related ${}^{3}J_{NC\gamma}$-coupling constants (through N–Cα–Cβ–Cγ) for ubiquitin using the experimental data reported by Hu and Bax (1997b). As shown in Fig. 2.10E and F, the experimental ${}^{3}J_{NC\gamma}$ data exhibited far better correlation with those calculated from the MD ensemble than with those calculated from the crystal structure. These results suggest that the χ_1 torsion angles of these hydrophilic side chains as well as the lysine χ_4 angles are as dynamic as seen in the MD simulation.

5.3. Hydrogen-bonding dynamics of lysine NH_3^+ groups

The NH_3^+ groups of Lys33, Lys48, and Lys63 exhibited relatively short bond-rotation correlation times τ_f (Table 2.3). This is consistent with the fact that they do not form hydrogen bonds with other parts of the protein in the crystal structure (Lys33 forms hydrogen bonds with a 41% occupancy in MD simulations). On the other hand, the NH_3^+ groups of Lys11, Lys27, and Lys29 exhibited relatively long bond-rotation correlation times τ_f (Table 2.3), suggesting that the motions of these NH_3^+ groups are restricted by hydrogen bond(s) with other protein parts. In fact, the crystal structures and MD simulations show hydrogen bonds involving these lysine residues. Table 2.4 lists intramolecular hydrogen bonds involving lysine NH_3^+ groups found in the 1 μs MD simulation. Their occupancies and average lifetimes in the trajectory are also shown. Some of them are not seen in the crystal structure, which is consistent with their occupancies in the trajectory well below 50%. The lifetimes of the intramolecular hydrogen bonds involving NH_3^+ groups are comparable to or shorter than the corresponding correlation times of the NH_3^+ bond rotations determined by NMR (Table 2.3). Thus both the MD simulation and NMR data suggest that hydrogen bonding by lysine NH_3^+ groups is highly dynamic with a subnanosecond lifetime. These results also suggest that the bond-rotation correlation times τ_f provide useful information about the timescale of hydrogen-bonding dynamics involving lysine NH_3^+ groups.

Hydrogen-bond scalar couplings ${}^{h3}J_{N\zeta C'}$ also provided direct insight into hydrogen bonds involving the lysine side chains of ubiquitin. Figure 2.11A

Table 2.4 Hydrogen bonds involving lysine NH_3^+ groups found in the MD simulation for ubiquitin with an occupancy higher than 25%

Donor	Acceptor	Presence in 1UBQ[a]	Occupancy[b] (%)	Average lifetime[c] (ps)
Lys11 Nζ	Glu34 Oε	Yes	62	20
Lys27 Nζ	Asp52 Oδ	Yes	72	24
Lys27 Nζ	Pro38 O	No	26	15
Lys29 Nζ	Glu16 O	Yes	64	31
Lys29 Nζ	Asp21 Oδ	No	36	60
Lys33 Nζ	Thr14 O	No	41	19

[a]PDB coordinates of 1.8 Å crystal structure of ubiquitin.
[b]Probability of the presence of a hydrogen bond in the MD trajectory.
[c]Average lifetime of a hydrogen bond. Equivalent atoms (i.e., three hydrogen atoms in an NH_3^+ group and two oxygen atoms in a side-chain carboxyl group) were distinguished in the calculation of lifetimes, whereas they were not distinguished in the calculation of occupancies.
Adapted from Esadze et al. (2011) with permission from the American Chemical Society.

shows the long-range correlation spectrum recorded to observe signals arising from the coherence transfers via $^{h3}J_{N\zeta C'}$ (with the pulses sequence in Fig. 2.6A). Such signals were clearly observed for Lys29 and Lys33 NH_3^+ groups. The ^{13}C chemical shifts for the signals observed for Lys29 and Lys33 NH_3^+ groups are in excellent agreement with those of backbone C═O groups of Glu16 and Thr14, respectively, which are in close proximity to the Nζ atoms in the crystal structure. Using the spin-echo $^{h3}J_{N\zeta C'}$-modulation difference constant-time HISQC experiment (Fig. 2.6B), the values of the $^{h3}J_{N\zeta C}$ constants for the lysine NH_3^+ groups were determined to be 0.23 Hz for the Lys29–Glu16 hydrogen bond and 0.17 Hz for the Lys33–Thr14 bond (Fig. 2.11B). These values are relatively small as compared to $^{h3}J_{NC'}$ constants for hydrogen bonds between backbone N—H and C═O groups, which can reach 0.9 Hz (Cordier & Grzesiek, 1999; Cornilescu, Hu, & Bax, 1999; Cornilescu et al., 1999; Grzesiek et al., 2004; Wang et al., 1999). The observed $^{h3}J_{N\zeta C'}$ couplings unequivocally indicate the presence of the hydrogen bonds between the NH_3^+ and C═O groups. The order parameters S^2_{axis} for the NH_3^+ groups of Lys29 and Lys33 (Table 2.3) indicate high mobility on the sub-nanosecond timescale. As shown in Fig. 2.11C and D, the MD simulation also shows a dynamic hydrogen-bonding process on a sub-nanosecond timescale for Lys29 and Lys33 side chains. These data together with the

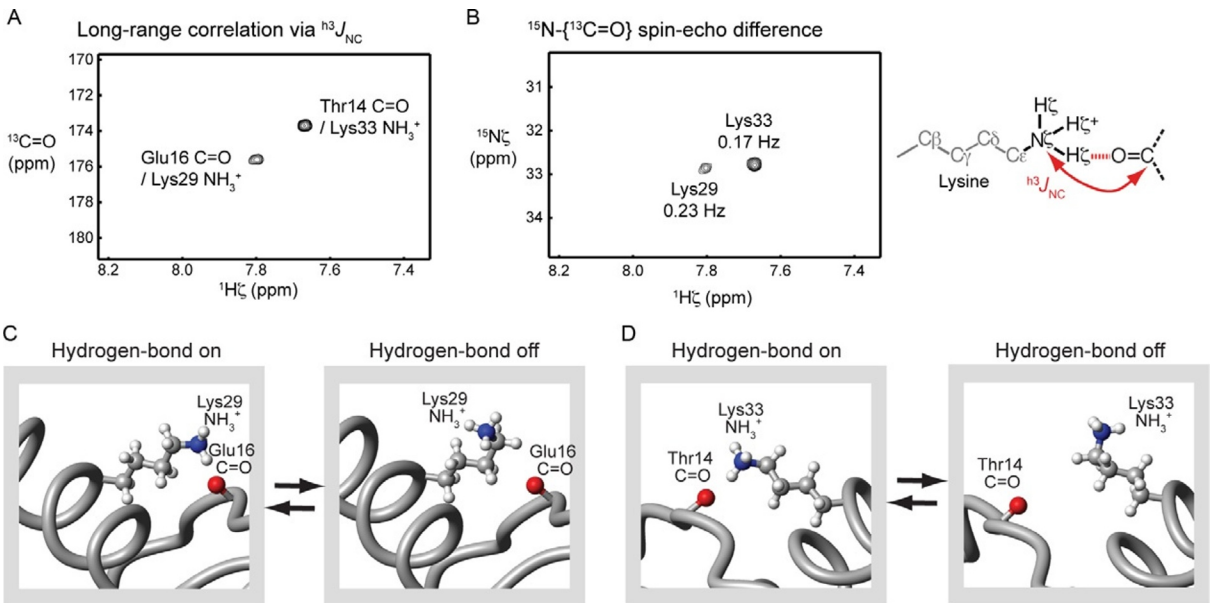

Figure 2.11 (A) Long-range correlations via $^{h3}J_{N\zeta C'}$ across a hydrogen bond $NH_3^+\cdots O{=}C$. This spectrum was recorded using the pulse sequence shown in Fig. 2.6A. (B) Spin-echo $^{h3}J_{N\zeta C'}$-modulation difference spectrum for the two sub-spectra recorded with the $^{13}C{=}O$ selective pulses at positions a and b in the pulse sequence shown in Fig. 2.6B. (C and D) Hydrogen-bonding dynamics of Lys29–Glu16 (C) and Lys33–Thr14 (D) hydrogen bonds seen in a 1000 ns MD simulation at 275 K. The acceptors are backbone carbonyl groups. These hydrogen bonds are experimentally confirmed by means of $^{h3}J_{N\zeta C'}$ (A and B). The average lifetimes of the hydrogen bonds in the MD simulation are 45 and 30 ps for Lys29 and Lys33, respectively. *Adapted from Zandarashvili et al. (2011) with permission from the American Chemical Society.*

detected $^{h3}J_{N\zeta C'}$ couplings collectively suggest that the hydrogen bonds of the lysine side chains are highly mobile.

6. ION-PAIR DYNAMICS INVOLVING LYSINE SIDE CHAINS AND THEIR ROLE IN PROTEIN–DNA ASSOCIATION

6.1. Contact ion-pair (CIP) and solvent-separated ion-pair (SIP) states

Ion pairing is one of the most fundamental atomic interactions in both chemistry and biology. In solution, one distinguishes two major states of ion pairs: contact ion pairs (CIP) and solvent-separated ion pairs (SIP) (Collins, 1997; Macchioni, 2005; Marcus & Hefter, 2006; Szwarc, 1969). In the CIP state, a cation and an anion are in direct contact with each other, whereas, in the SIP state, there are one or more solvent molecules between the electrostatically interacting cation and anion (Fig. 2.12). In previous studies, ion-pair dynamics of small organic compounds were characterized experimentally using time-resolved absorption spectroscopy, infrared spectroscopy, and Raman spectroscopy (Masnovi & Kochi, 1985; Peters & Li, 1994; Simon & Peters, 1982; Yabe & Kochi, 1992). The transitions between the CIP and SIP states were found to occur on a ps–ns timescale for the ion pairs of these small organic compounds, and the free energy differences between their CIP and SIP states were found to be ~1–2 kcal mol^{-1} (Lü et al., 2005; Masnovi & Kochi, 1985; Peters & Li, 1994; Simon & Peters, 1982; Yabe & Kochi, 1992). Despite the wealth of information available for small organic compounds, very little is currently known about the dynamics of ion pairs tethered to biological macromolecules because their

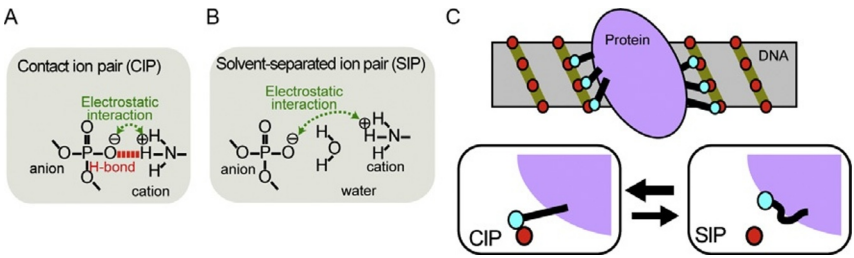

Figure 2.12 Two major states for an ion pair. (A) The CIP state. (B) The SIP state. (C) Transitions between the CIP and SIP states for interfacial ion pairs between protein and DNA.

complexity renders application of the traditional methods impractical. Very recently, the methodological progress in NMR spectroscopy, which is described in Sections 3 and 4, has led to a breakthrough in this field.

6.2. Mobility of Lys NH_3^+ groups in ion pairs with DNA

Using the NMR methods described in Sections 3 and 4, Anderson et al. studied the ion-pair dynamics at protein–DNA interface for two DNA complexes of HoxD9 homeodomain (Anderson et al., 2013): One with a normal 24 bp DNA duplex ("Complex I"), and the other with a modified 24 bp DNA duplex containing a phosphorodithioate group instead of the phosphate group that forms an ion pair with Lys57 ("Complex II") (Fig. 2.13). In HISQC spectra, $^1H—^{15}N$ cross-peaks of side-chain NH_3^+ groups of Lys3, Lys55, and Lys57 were observed for both complexes at pH 5.8 and 35 °C. As shown in Fig. 2.13A, the oxygen-to-sulfur substitution in the ion pair with Lys57 caused large perturbations in ^1H and ^{15}N resonances of the Lys57 NH_3^+ group. Signals from Lys3 and Lys55 NH_3^+ groups remained almost unchanged, which is not surprising because the location of the dithioation is specifically on the phosphate group interacting with Lys57.

For the Lys NH_3^+ groups of Complexes I and II, ^{15}N relaxation rates R_1, R_2, and $R(4N_zH_zH_z)$ and $^1H—^{15}N$ NOE were measured. From the relaxation data, order parameters for the amino group symmetry axis S^2_{axis}, C—N bond-rotation correlation times τ_f, and reorientational correlation times τ_i were determined for the Lys NH_3^+ groups at the protein–DNA interface (Table 2.5). Interestingly, the order parameters S^2_{axis} of Lys NH_3^+ groups interacting with DNA were smaller than 0.5, indicating that the ion pairs between Lys side-chain NH_3^+ and DNA phosphate groups are highly mobile despite the simultaneous presence of the hydrogen-bonding and short-range electrostatic interactions in the ion pairs. The dynamic nature of the interfacial ion pairs should be favorable for protein–DNA association because it should minimize the loss of conformational entropy from immobilization of side chains upon the formation of the complex.

6.3. Hydrogen-bonding dynamics of the interfacial ion pairs

To obtain information on the CIP and SIP states, Anderson et al. also studied hydrogen-bond scalar couplings $^{h3}J_{NP}$ between Lys side-chain ^{15}N and DNA ^{31}P nuclei in the ion pairs at the protein–DNA interface. Note that the CIP state can exhibit $^{h3}J_{NP}$ coupling, whereas the SIP state cannot

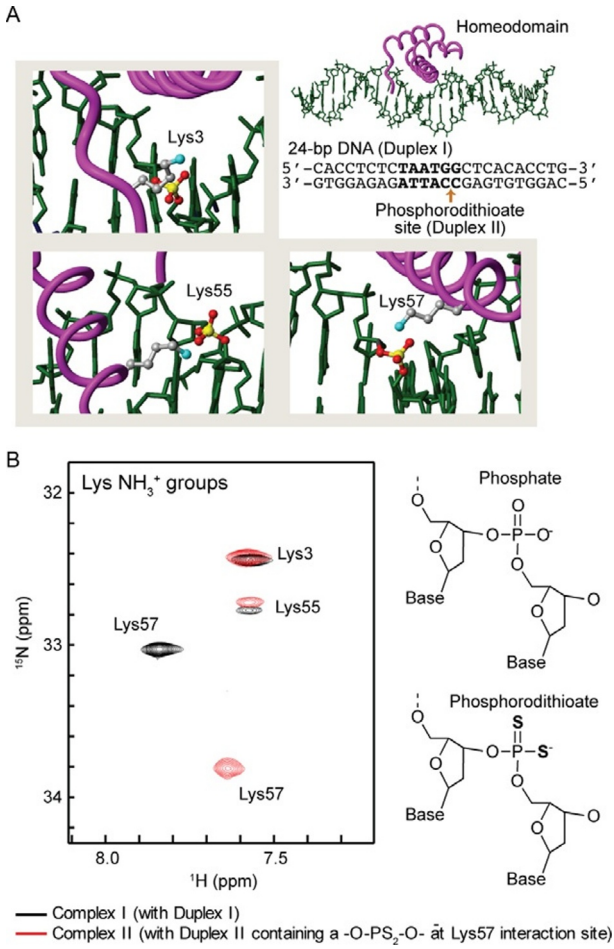

Figure 2.13 Interfacial ion pairs involving Lys NH_3^+ groups studied by NMR (Anderson et al., 2013). (A) Intermolecular ion pairs involving Lys side-chain NH_3^+ groups and DNA phosphate or phosphorodithioate groups studied in this work. Two 24 bp DNA duplexes with the same sequence (the recognition site in bold) were used: Duplex I with no chemical modification; and Duplex II with a phosphorodithioate incorporated at the position of the ion pair with Lys57. (B) Overlaid HISQC spectra of the Lys NH_3^+ groups recorded for HoxD9 homeodomain complexes with Duplex I and with Duplex II at 35 °C.*Adapted from Anderson et al. (2013) with permission from the American Chemical Society.*

(Fig. 2.12). Spectra recorded by this experiment for Complexes I and II clearly show intermolecular $^1H—^{31}P$ correlation signals (Fig. 2.14A–C), indicating at least part-time presence of the CIP states for the ion pairs between Lys NH_3^+ and DNA phosphate/phosphorodithioate groups.

Table 2.5 ^{15}N relaxation and dynamics parameters for the Lys side-chain NH_3^+ groups in the intermolecular ion pairs in the HoxD9 homeodomain–DNA complexes at 35 °C

	Lys3 NH_3^+	Lys55 NH_3^+	Lys57 NH_3^+
Complex I [a]			
800 MHz			
^{15}N R_1 (s^{-1})	0.25 ± 0.01	0.43 ± 0.02	0.74 ± 0.01
^{15}N $R_{2,ini}$ (s^{-1})[b]	0.98 ± 0.05	1.98 ± 0.21	2.27 ± 0.04
^{1}H—^{15}N NOE	-2.40 ± 0.03	-2.72 ± 0.08	-3.00 ± 0.03
600 MHz			
^{15}N R_1 (s^{-1})	0.27 ± 0.01	0.59 ± 0.04	0.80 ± 0.02
^{1}H—^{15}N NOE	-3.07 ± 0.06	-2.94 ± 0.17	-3.17 ± 0.04
Dynamics[c]			
S^2_{axis}	0.22 ± 0.02	0.46 ± 0.06	0.48 ± 0.01
τ_f (ps)	3 ± 1	23 ± 2	113 ± 42
τ_i (ps)	222 ± 16	249 ± 42	82 ± 132
Complex II [d]			
800 MHz			
^{15}N R_1 (s^{-1})	0.29 ± 0.02	0.43 ± 0.03	0.33 ± 0.02
^{15}N $R_{2,ini}$ (s^{-1})[b]	1.16 ± 0.07	2.18 ± 0.26	1.76 ± 0.05
^{1}H—^{15}N NOE	-2.63 ± 0.06	-2.72 ± 0.09	-3.02 ± 0.13
600 MHz			
^{15}N R_1 (s^{-1})	0.29 ± 0.02	0.54 ± 0.08	0.36 ± 0.02
^{1}H—^{15}N NOE	-3.24 ± 0.10	-3.08 ± 0.20	-3.08 ± 0.13
Dynamics[c]			
S^2_{axis}	0.26 ± 0.02	0.49 ± 0.06	0.39 ± 0.01
τ_f (ps)	8 ± 4	26 ± 12	27 ± 7
τ_i (ps)	163 ± 43	184 ± 87	36 ± 19

[a]With Duplex I (see Fig. 2.13).
[b]The initial rate for intrinsically biexponential ^{15}N transverse relaxation[13] of NH_3^+.
[c]Symbols are defined in Fig. 2.4. The molecular rotational correlation time and anisotropy were determined to be 10.6 ns and 2.1, respectively, from backbone ^{15}N relaxation data.
[d]With Duplex II that contains a phosphorodithioate group at the ion pair with Lys57.
Adapted from Anderson et al. (2013) with permission from the American Chemical Society.

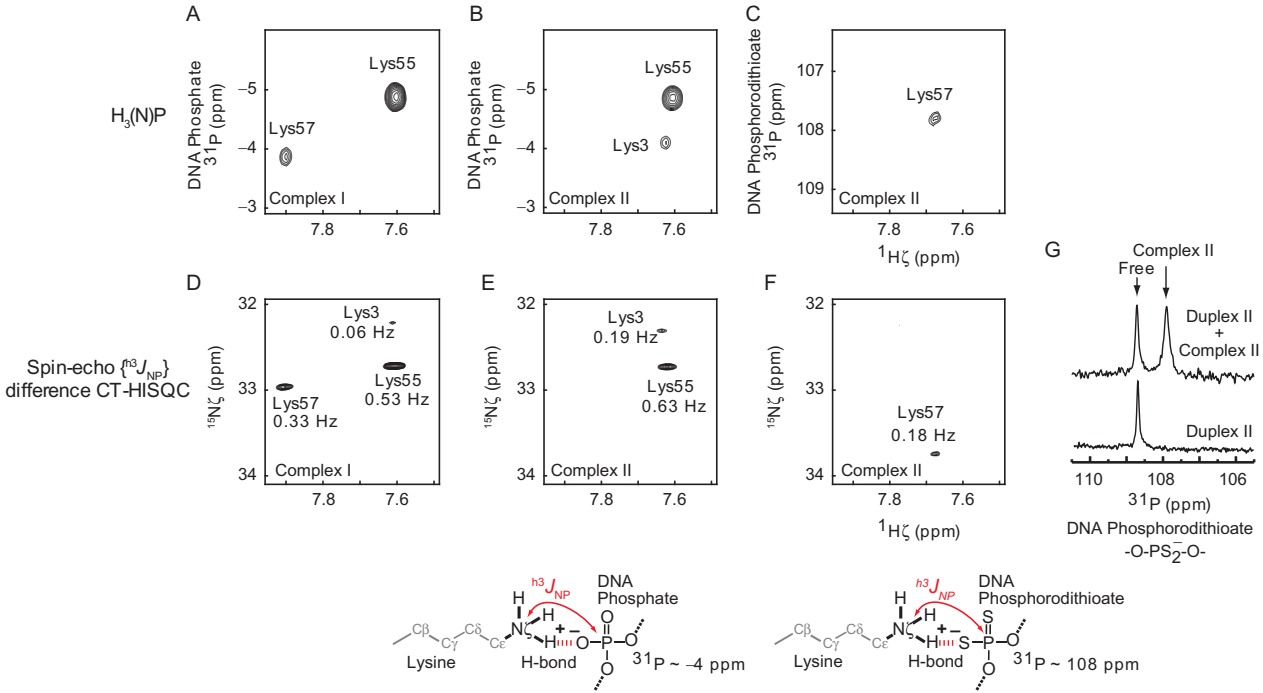

Figure 2.14 Hydrogen-bond scalar $^{15}N—^{31}P$ coupling $^{h3}J_{NP}$ between ^{15}N and ^{31}P nuclei as evidenced for the presence of CIP in the HoxD9 homeodomain–DNA complexes I and II (Anderson et al., 2013). (A–C) 2D $H_3(N)P$ spectra that give heteronuclear $^{1}H—^{31}P$ correlation cross-peaks via $^{h3}J_{NP}$ coupling. (D–F) Difference spectra recorded by the spin-echo $^{h3}J_{NP}$-modulation constant-time HISQC experiment. Measured absolute values of $^{h3}J_{NP}$ are also indicated. Percentage errors were estimated to be less than 20%. ^{31}P carrier positions were set to −3 ppm for panels (A), (B), (D), and (E) (for DNA phosphate); and 107 ppm for panels (C) and (F) (for DNA phosphorodithioate). The pulse sequences are shown in Fig. 2.6C and D. (G) Phosphorodithioate regions of 1D ^{31}P spectra recorded for Duplex II in the free state and a mixture of Duplex II and Complex II. ^{31}P chemical shift of the cross-peak in panel (C) agrees with ^{31}P chemical shift of the signal from Complex II in the panel (G). ^{1}P chemical shifts are relative to trimethylphosphate (TMP). *Adapted from Anderson et al. (2013) with permission from the American Chemical Society.*

Observed ^{31}P chemical shifts for DNA phosphates in the ion pairs with Lys55 (−4.88 ppm) and Lys57 (−3.86 ppm) lie at the outer edges of typical ^{31}P chemical shifts (−4.8 to −3.9 ppm) for B-form DNA (Gorenstein, 1994), presumably due to ion pairing effects. ^{31}P chemical shift of the phosphorodithioate group in the ion pair with Lys57 was found to be 117.78 ppm (Fig. 2.14C), which was confirmed with 1D ^{31}P NMR (Fig. 2.14G).

To determine the absolute values of $^{h3}J_{NP}$ coupling constants, the spin-echo $^{h3}J_{NP}$-modulation constant-time HISQC experiment was designed (the pulse sequence shown in Fig. 2.6C and D). Using signal intensities in the two sub-spectra recorded by this experiment, Anderson et al. determined the absolute values of the $^{h3}J_{NP}$ coupling constants for the intermolecular ion pairs in Complexes I and II to range from 0.06 to 0.63 Hz (Fig. 2.14D–F). For Lys55 and Lys57 NH_3^+ groups, crystal structures of highly homologous protein–DNA complexes exhibit the CIP states of their ion pairs with DNA. From the crystal structures, $^{h3}J_{NP}$ coupling constants for these NH_3^+ groups were predicted with the density functional theory (DFT) method. The experimental $^{h3}J_{NP}$ constants were comparable to the averages of the predicted constants, suggesting that the CIP state has a major presence in solution for the ion pairs of Lys55 and Lys57 NH_3^+ groups with a DNA phosphate group. The $^{h3}J_{NP}$ coupling for phosphorodithioate–Lys57 NH_3^+ ion pair (0.18 Hz) was found to be significantly smaller than that for phosphate–Lys57 NH_3^+ ion pair (0.33 Hz). On the contrary, DFT calculations suggested that $|^{h3}J_{NP}|$ of phosphorodithioate tends to be larger for the same hydrogen-bonding geometry. The observed small $|^{h3}J_{NP}|$ for the phosphorodithioate–Lys57 NH_3^+ ion pair could be partly due to the higher degree of dynamics that ^{15}N relaxation data indicate.

The experimental and computational $^{h3}J_{NP}$ coupling data suggest a major presence of CIP for the intermolecular ion pairs involving Lys55 and Lys57 NH_3^+ groups. This is consistent with the finding that C—N bond-rotation correlation times τ_f of these NH_3^+ groups are clearly slower than that of the Lys3 NH_3^+ group (Table 2.5). Hydrogen bonds with phosphate/phosphorodithioate in the CIP state should render slower bond rotations of Lys55 and Lys57 NH_3^+ groups. Transient breakage of the hydrogen bonds can be accompanied by rotational permutations of hydrogen atoms within the CIP state or a transition to SIP. Given the major presence of CIP, it is likely that the timescale of the transient hydrogen-bond breakage for Lys55 and Lys57 NH_3^+ groups is faster than or comparable to their bond-rotation correlation times τ_f (see Section 4.2). The τ_f data suggest that the transient

breakage of hydrogen bonds between Lys NH_3^+ and DNA phosphate/phosphorodithioate groups occurs on a sub-nanosecond timescale.

The faster C—N bond rotation of the Lys3 NH_3^+ group implicates a higher population of the SIP state with no hydrogen bonds with DNA. The τ_f values for the Lys3 NH_3^+ group in Complexes I and II are smaller than those (~25 ps) for Lys NH_3^+ groups that do not form any hydrogen bond in ubiquitin at 2 °C (Esadze et al., 2011), but the higher temperature (35 °C) in the study of the HoxD9–DNA complexes can explain this discrepancy. The Lys3 side chain is disordered in all of the crystal structures of homeodomain–DNA complexes except one (PDB 1IG7). The only structure available for the Lys3 side chain shows that the ion pair between Lys3 and DNA is in the SIP state with an Nζ···OP distance of 5.4 Å, although simple rotation about χ_3 can reduce this distance to ~3.0 Å. On the other hand, weak $^{h3}J_{NP}$ coupling was observed for Lys3 (Fig. 2.14B, D, E), which indicates at least a part-time presence of the CIP. The small $|^{h3}J_{NP}|$, short τ_f, and small S^2_{axis} collectively suggest a low population of the CIP state for the ion pair of the Lys3 NH_3^+ group. Thus, the equilibrium between the CIP and SIP states (Fig. 2.12C) for Lys3 appears to be shifted toward the SIP, while the corresponding equilibria for Lys55 and Lys57 appear to be shifted toward the CIP.

6.4. How can dithioation of DNA phosphate enhance protein–DNA association?

Although it is well known that oxygen-to-sulfur substitution in DNA phosphate can enhance protein–DNA interactions (Cummins, Graff, Beaton, Marshall, & Caruthers, 1996; King et al., 2002; King, Ventura, Brasier, & Gorenstein, 1998; Marshall & Caruthers, 1993), the mechanism is not well understood. The protein–DNA affinity enhancement by the oxygen-to-sulfur substitution may appear counterintuitive to chemists, given the fact that sulfur atoms in organic compounds tend to serve as relatively poor hydrogen-bond acceptors. For example, the boiling point of methanethiol (CH_3SH) is lower by 59 °C than that of methanol (CH_3OH); and the boiling point of 2-mercaptoethanol (HO–CH_2–CH_2–SH) is lower by 40 °C than that of ethylene glycol (HO–CH_2–CH_2–OH). Despite this nature of sulfur, how can oxygen-to-sulfur substitution in DNA phosphate enhance protein–DNA association? The NMR data of Anderson et al. (2013) provide new insights into this interesting phenomenon.

The S^2_{axis} data indicate that the Lys57 NH_3^+ group in the ion pair with a phosphorodithioate group is more mobile than in the ion pair with a

phosphate group (Table 2.5). Interestingly, the C—N bond-rotation correlation time τ_f is significantly faster for the Lys57 NH_3^+ group in the ion pair with a phosphorodithioate group. This causes substantially different ^{15}N R_1 rates of Lys57 NH_3^+ groups in Complexes I and II (Fig. 2.15A; see also Table 2.5). The higher mobility of the ion pair with a phosphorodithioate group is consistent with the two facts that (1) the effective ionic radius of sulfur (1.84 Å) is substantially larger than that of oxygen (1.40 Å), and that

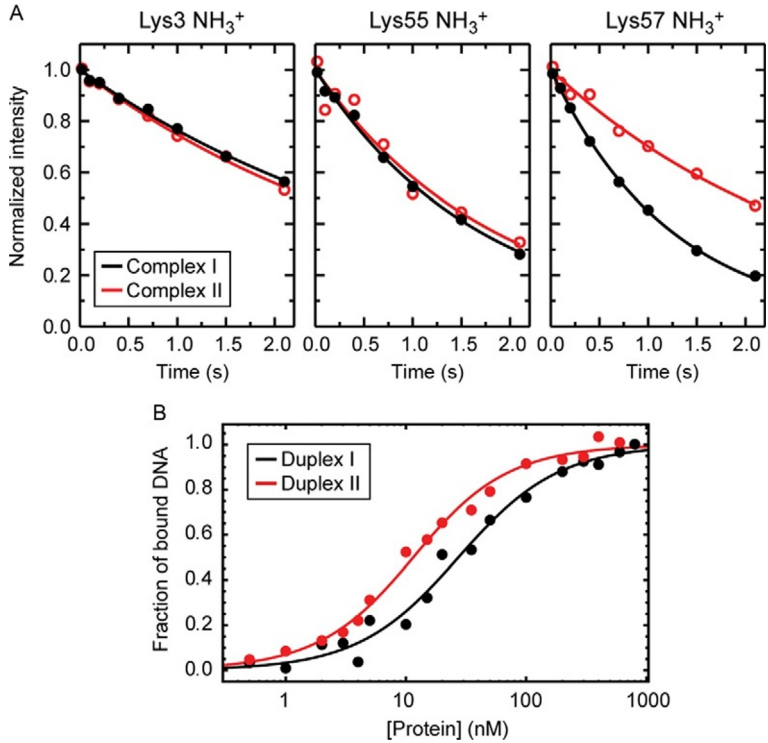

Figure 2.15 Influence of the oxygen-to-sulfur substitution in the DNA phosphate group interacting with Lys57 in the HoxD9 homeodomain–DNA complex (Anderson et al., 2013). (A) ^{15}N longitudinal relaxation of Lys side-chain NH_3^+ groups at the protein–DNA interfaces of Complexes I and II. Lys57 NH_3^+ group exhibited substantially different relaxation upon the oxygen-to-sulfur substitution in the DNA phosphate group. ^{15}N relaxation of the other NH_3^+ groups (interacting with normal phosphate group in both complexes) was virtually unaffected. (B) Binding isotherm as monitored with fluorescence arising from a rhodamine attached to the 5′-terminus of DNA. Fractions of bound DNA calculated from the fluorescence anisotropy data at varying concentrations of HoxD9 homeodomain are plotted for Duplexes I and II. *Adapted from Anderson et al. (2013) with permission from the American Chemical Society.*

(2) the potential energy surface for an H···S hydrogen bond is flatter than that for an H···O hydrogen bond (Wennmohs, Staemmler, & Schindler, 2003). Due to the flatter energy surface, on which a slight deviation from ideal hydrogen-bond geometry causes only a marginal increase in enthalpy, a donor of a H···S hydrogen bond should be able to take up a wider space without significant enthalpic loss. Based on the experimental order parameters S^2_{axis} and the C—N bond-rotation correlation times τ_f for Lys57 NH_3^+ groups in Complexes I and II, Anderson et al. estimated that the overall increase of entropy (i.e., reorientational + rotational) by mobilizing the NH_3^+ group is thus estimated to be ~ 0.8 cal mol^{-1} K^{-1} (Anderson et al., 2013).

This mobilization of the ion pair can at least partially explain affinity enhancement of the protein–DNA association by the oxygen-to-sulfur substitution. The affinity of Duplex II was found to be threefold higher than that of Duplex I (Fig. 2.15B); the dissociation constants (K_d) were determined to be 31 ± 6 nM for Complex I and 12 ± 4 nM for Complex II. From the K_d data, the difference between the binding free energies ($\Delta\Delta G = \Delta G_{II} - \Delta G_I$) is calculated to be -0.6 kcal mol^{-1}. The major contributor to this $\Delta\Delta G$ should be the entropy term (i.e., $-T\Delta\Delta S$), because recent theoretical quantum chemical studies showed that the enthalpy ΔH for H···S hydrogen bonds is slightly smaller than that for H···O hydrogen bonds (Howard & Kjaergaard, 2008; Wennmohs et al., 2003). In fact, the entropic term for mobilization of the NH_3^+ group alone corresponds to -0.24 kcal mol^{-1} at 20 °C. If the entropic effect for the other parts of the ion pair (e.g., methylene groups of the Lys side chain) is comparable to this, the observed $\Delta\Delta G$ can be explained in terms of the enhanced ion-pair dynamics, although other factors (e.g., different desolvation energies) may also contribute.

7. CONCLUSIONS AND FUTURE PERSPECTIVES

As described above, the new NMR methods along with the computational/theoretical approaches have provided important insights into protein side-chain dynamics involving hydrogen bonds and ion pairs. One of the most important findings from these studies is that hydrogen bonds and ion pairs involving lysine side chains are remarkably dynamic. For example, despite the simultaneous presence of the short-range electrostatic interaction and hydrogen bonding, the ion pairs between protein and DNA are highly dynamic as reflected in the low order parameters of lysine NH_3^+ groups. The bond-rotation and reorientation correlation times suggest that

breakage of side-chain hydrogen bonds occurs on a sub-nanosecond timescale. The high degree of flexibility of the intermolecular ion pairs should minimize the side-chain conformational entropic costs for protein–DNA association. The oxygen-to-sulfur substitution in DNA phosphate makes the intermolecular ion pair more dynamic, which seems to contribute to the affinity enhancement by this type of substitution.

Owing to the very slow ^{15}N transverse relaxation of NH_3^+ groups, which is even slower than ^{13}C transverse relaxation of CH_3 groups, NH_3^+ groups can be used as very sensitive probes that are suitable for the NMR investigations of large proteins or protein complexes, provided that hydrogen exchange is slow enough. Although direct ^1H observation of NH_3^+ groups requires a relatively low pH (~5-6), this does not diminish biological relevance of the investigations for proteins that retain their activities at such a pH. It should also be noted that there are many proteins for which low pH is biologically important; for example, those in lysosome or vacuole cell organelles (pH ~5) (Voet & Voet, 2004) and enzymes secreted in digestive organs. Applications of the methodology can be further extended to characterizations of lysine side-chain amino groups at catalytic sites of the enzymes, and at other sites crucial for protein functions. New insights from such characterizations will help deepen our understanding of the role of side-chain dynamics in protein functions. This methodology can also address impact of salt on protein function in terms of the side-chain dynamics. Modulation of ionic strength is known to affect macromolecular kinetics and thermodynamics, although atomic details about this phenomenon are not known. Thus, there are many potential applications in biophysics, protein chemistry, and structural biology.

Finally, we should mention that the experimental data on the hydrogen-bonding dynamics and ion-pair dynamics also allow the computational biology community to validate and even improve the MD force fields. Because of the empirical nature of the force-field parameters, it is important to examine agreement between the computational and experimental results. Experiment-based improvement of the force-field parameters can ultimately lead to advances in drug design and protein engineering for human therapeutics.

ACKNOWLEDGMENT

This work was supported by Grant 12BGIA8960032 from the American Heart Association and by Grant CHE-1307344 from the National Science Foundation. We thank Drs Rafael Brüschweiler, David Gorenstein, Da-Wei Li, Tianzhi Wang, and Kurtis Anderson for collaborating with us in the research on the dynamics of lysine NH_3^+ groups in the past few years.

REFERENCES

Abragam, A. (1961). *The Principles of Nuclear Magnetism*. Oxford: Carendon Press, 309.

Anderson, K. M., Esadze, A., Manoharan, M., Bruschweiler, R., Gorenstein, D. G., & Iwahara, J. (2013). Direct observation of the ion-pair dynamics at a protein-DNA interface by NMR spectroscopy. *Journal of the American Chemical Society*, *135*(9), 3613–3619.

Andre, I., Linse, S., & Mulder, F. A. (2007). Residue-specific pKa determination of lysine and arginine side chains by indirect ^{15}N and 13C NMR spectroscopy: application to apo calmodulin. *Journal of the American Chemical Society*, *129*(51), 15805–15813.

Baldwin, A. J., Hansen, D. F., Vallurupalli, P., & Kay, L. E. (2009). Measurement of methyl axis orientations in invisible, excited states of proteins by relaxation dispersion NMR spectroscopy. *Journal of the American Chemical Society*, *131*(33), 11939–11948.

Bandyopadhyay, S., Chakraborty, S., & Bagchi, B. (2005). Secondary structure sensitivity of hydrogen bond lifetime dynamics in the protein hydration layer. *Journal of the American Chemical Society*, *127*(47), 16660–16667.

Bax, A. (2003). Weak alignment offers new NMR opportunities to study protein structure and dynamics. *Protein Science*, *12*(1), 1–16.

Bax, A., Ikura, M., Kay, L. E., Torchi, D. A., & Tschudin, R. (1990). Comparison of different modes of two-dimensional reverse-correlation NMR for the study of proteins. *Journal of Magnetic Resonance*, *86*, 304–318.

Bax, A., Vuister, G. W., Grzesiek, S., Delaglio, F., Wang, A. C., Tschudin, R., et al. (1994). Measurement of homo- and heteronuclear J couplings from quantitative J correlation. *Methods in Enzymology*, *239*, 79–105.

Bhoj, V. G., & Chen, Z. J. (2009). Ubiquitylation in innate and adaptive immunity. *Nature*, *458*(7237), 430–437.

Brown, L. R., De Marco, A., Wagner, G., & Wuthrich, K. (1976). A study of the lysyl residues in the basic pancreatic trypsin inhibitor using 1H nuclear magnetic resonance at 360 Mhz. *European Journal of Biochemistry*, *62*(1), 103–107.

Brüschweiler, R., & Wright, P. E. (1994). NMR order parameters of biomolecules—A new analytical representation and application to the Gaussian axial fluctuation model. *Journal of the American Chemical Society*, *116*(18), 8426–8427.

Burke, T. E. (1970). Nuclear spin relaxation in the presence of internal rotation. II. Nuclear-spin-internal-rotational coupling in benzotrifluoride and hexafluorobutyne-2. *Journal of Magnetic Resonance*, *2*, 120–140.

Carr, H. Y., & Purcell, E. M. (1954). Effects of diffusion on free precession in nuclear magnetic resonance experiments. *Physical Review*, *94*, 630–638.

Cavanagh, J., Fairbrother, W. J., Palmer, A. G., III., Rance, M., & Skelton, N. J. (2007). *Protein NMR sprectroscopy: principles and practice* (2 ed.). Burlignton: Elsevier Academic Press.

Clore, G. M., & Iwahara, J. (2009). Theory, practice, and applications of paramagnetic relaxation enhancement for the characterization of transient low-population states of biological macromolecules and their complexes. *Chemical Review*, *109*(9), 4108–4139.

Collins, K. D. (1997). Charge density-dependent strength of hydration and biological structure. *Biophysical Journal*, *72*(1), 65–76.

Cordier, F., & Grzesiek, S. (1999). Direct observation of hydrogen bonds in proteins by interresidue (3h)J(NC') scalar couplings. *Journal of the American Chemical Society*, *121*(7), 1601–1602.

Cornilescu, G., Hu, J. S., & Bax, A. (1999). Identification of hydrogen bonding network in a protein by scalar couplings. *Journal of the American Chemical Society*, *121*, 2949–2950.

Cornilescu, G., Rzmirez, B. E., Frank, M. K., Clore, G. M., Gronenborn, A. M., & Bax, A. (1999). Correlation between 3hJNC′ and hydrogen bond length in proteins. *Journal of the American Chemical Society*, *121*, 6275–6279.

Cummins, L., Graff, D., Beaton, G., Marshall, W. S., & Caruthers, M. H. (1996). Biochemical and physicochemical properties of phosphorodithioate DNA. *Biochemistry*, *35*(26), 8734–8741.

Englander, S. W., Downer, N. W., & Teitelbaum, H. (1972). Hydrogen exchange. *Annual Review of Biochemistry*, *41*, 903–924.

Esadze, A., Li, D. W., Wang, T., Brüschweiler, R., & Iwahara, J. (2011). Dynamics of lysine side-chain amino groups in a protein studied by heteronuclear ^{1}H-^{15}N NMR spectroscopy. *Journal of the American Chemical Society*, *133*, 909–919.

Farrow, N. A., Zhang, O., Forman-Kay, J. D., & Kay, L. E. (1994). A heteronuclear correlation experiment for simultaneous determination of 15N longitudinal decay and chemical exchange rates of systems in slow equilibrium. *Journal of Biomolecular NMR*, *4*(5), 727–734.

Fushman, D., & Walker, O. (2010). Exploring the linkage dependence of polyubiquitin conformations using molecular modeling. *Journal of Molecular Biology*, *395*(4), 803–814.

Gao, G., DeRose, E. F., Kirby, T. W., & London, R. E. (2006). NMR determination of lysine pKa values in the Pol lambda lyase domain: Mechanistic implications. *Biochemistry*, *45*(6), 1785–1794.

Gao, G., Prasad, R., Lodwig, S. N., Unkefer, C. J., Beard, W. A., Wilson, S. H., et al. (2006). Determination of lysine pK values using [5-13C]lysine: Application to the lyase domain of DNA Pol beta. *Journal of the American Chemical Society*, *128*(25), 8104–8105.

Gorenstein, D. G. (1994). Conformation and dynamics of DNA and protein-DNA complexes by ^{31}P NMR. *Chemical Review*, *94*(5), 1315–1338.

Grzesiek, S., & Bax, A. (1993). The importance of not saturating H_2O in protein NMR. Application to sensitivity enhancement and NOE measurements. *Journal of the American Chemical Society*, *115*, 12593–12594.

Grzesiek, S., Cordier, F., Jaravine, V., & Barfield, M. (2004). Insights into biomolecular hydrogen bonds from hydrogen bond scalar couplings. *Progress in Nuclear Magnetic Resonance Spectroscopy*, *45*(3–4), 275–300.

Hansen, D. F., Vallurupalli, P., & Kay, L. E. (2008). An improved 15N relaxation dispersion experiment for the measurement of millisecond time-scale dynamics in proteins. *The Journal of Physical Chemistry. B*, *112*(19), 5898–5904.

Hershko, A. (1997). Roles of ubiquitin-mediated proteolysis in cell cycle control. *Current Opinion in Cell Biology*, *9*(6), 788–799.

Hershko, A., & Ciechanover, A. (1992). The ubiquitin system for protein degradation. *Annual Review of Biochemistry*, *61*, 761–807.

Howard, D. L., & Kjaergaard, H. G. (2008). Hydrogen bonding to divalent sulfur. *Physical Chemistry Chemical Physics*, *10*(28), 4113–4118.

Hu, J. S., & Bax, A. (1997a). Chi 1 angle information from a simple two-dimensional NMR experiment that identifies trans 3JNC gamma couplings in isotopically enriched proteins. *Journal of Biomolecular NMR*, *9*(3), 323–328.

Hu, J. S., & Bax, A. (1997b). χ_1 angle information from a simple two-dimensional NMR experiment that identifies trans $^{3}J_{NC\gamma}$ couplings in isotopically enriched proteins. *Journal of Biomolecular NMR*, *9*(3), 323–328.

Idiyatullin, D., Daragan, V. A., & Mayo, K. H. (2001). Improved measurement of N-15-{H-1} NOEs in the presence of H(N)-water proton chemical exchange. *Journal of Magnetic Resonance*, *153*(1), 138–143.

Iwahara, J., Jung, Y. S., & Clore, G. M. (2007). Heteronuclear NMR spectroscopy for lysine NH_3 groups in proteins: Unique effect of water exchange on (15)N transverse relaxation. *Journal of the American Chemical Society*, *129*(10), 2971–2980.

Karplus, M. J. (1959). Contact electron-spin coupling of nuclear magnetic moments. *Journal of Chemical Physics*, *30*, 11–15.

Kay, L. E., Bull, T. E., Nicholson, L. K., Griesinger, C., Schwalbe, H., Bax, A., et al. (1992). The measurement of heteronuclear transverse relaxation-times in Ax3 spin systems via polarization-transfer techniques. *Journal of Magnetic Resonance*, *100*(3), 538–558.

Kay, L. E., & Torchia, D. A. (1991). The effects of dipolar cross-correlation on C-13 methyl-carbon T1, T2, and Noe measurements in macromolecules. *Journal of Magnetic Resonance*, *95*(3), 536–547.

King, D. J., Bassett, S. E., Li, X., Fennewald, S. A., Herzog, N. K., Luxon, B. A., et al. (2002). Combinatorial selection and binding of phosphorothioate aptamers targeting human NF-kappa B RelA(p65) and p50. *Biochemistry*, *41*(30), 9696–9706.

King, D. J., Ventura, D. A., Brasier, A. R., & Gorenstein, D. G. (1998). Novel combinatorial selection of phosphorothioate oligonucleotide aptamers. *Biochemistry*, *37*(47), 16489–16493.

Korzhnev, D. M., & Kay, L. E. (2008). Probing invisible, low-populated States of protein molecules by relaxation dispersion NMR spectroscopy: An application to protein folding. *Accounts of Chemical Research*, *41*(3), 442–451.

Kumar, A., Grace, R. C. R., & Madhu, P. K. (2000). Cross-correlations in NMR. *Progress in Nuclear Magnetic Resonance Spectroscopy*, *37*(3), 191–319.

Lakomek, N. A., Lange, O. F., Walter, K. F., Fares, C., Egger, D., Lunkenheimer, P., et al. (2008). Residual dipolar couplings as a tool to study molecular recognition of ubiquitin. *Biochemical Society Transactions*, *36*(Pt 6), 1433–1437.

Lehmann, M. S., Koetzle, T. F., & Hamilton, W. C. (1971). Precision neutron diffraction structure determination of protein and nucleic acid components. I. The crystal and molecular structure of the amino Acid L-alanine. *Journal of the American Chemical Society*, *94*(8), 2657–2660.

Li, Y. C., & Montelione, G. T. (1994). Overcoming solvent saturation-transfer artifacts in protein NMR at neutral pH—Application of pulsed-field gradients in measurements of H-1N-15 Overhauser effects. *Journal of Magnetic Resonance Series B*, *105*(1), 45–51.

Liepinsh, E., & Otting, G. (1996). Proton exchange rates from amino acid side chains—Implications for image contrast. *Magnetic Resonance in Medicine*, *35*(1), 30–42.

Lipari, G., & Szabo, A. (1982). Model-free approach to the interpretation of nuclear magnetic-resonance relaxation in macromolecules. 1. Theory and range of validity. *Journal of the American Chemical Society*, *104*(17), 4546–4559.

Loria, J. P., Berlow, R. B., & Watt, E. D. (2008). Characterization of enzyme motions by solution NMR relaxation dispersion. *Accounts of Chemical Research*, *41*(2), 214–221.

Loria, J. P., Rance, M., & Palmer, A. G. (1999). A relaxation-compensated Carr-Purcell-Meiboom-Gill sequence for characterizing chemical exchange by NMR spectroscopy. *Journal of the American Chemical Society*, *121*(10), 2331–2332.

Lü, J. M., Rosokha, S. V., Lindeman, S. V., Neretin, I. S., & Kochi, J. K. (2005). "Separated" versus "contact" ion-pair structures in solution from their crystalline states: dynamic effects on dinitrobenzenide as a mixed-valence anion. *Journal of the American Chemical Society*, *127*(6), 1797–1809.

Macchioni, A. (2005). Ion pairing in transition-metal organometallic chemistry. *Chemical Review*, *105*(6), 2039–2073.

Marcus, Y., & Hefter, G. (2006). Ion pairing. *Chemical Review*, *106*(11), 4585–4621.

Marshall, W. S., & Caruthers, M. H. (1993). Phosphorodithioate DNA as a potential therapeutic drug. *Science*, *259*(5101), 1564–1570.

Masnovi, J. M., & Kochi, J. K. (1985). Direct observation of ion-pair dynamics. *Journal of the American Chemical Society*, *107*(26), 7880–7893.

Meiboom, S., & Gill, D. (1958). *The Review of Scientific Instruments*, *29*, 688–691.

Ollerenshaw, J. E., Tugarinov, V., & Kay, L. E. (2003). Methyl TROSY: Explanation and experimental verification. *Magnetic Resonance in Chemistry*, *41*(10), 843–852.

Palmer, A. G., 3rd. (2001). NMR probes of molecular dynamics: Overview and comparison with other techniques. *Annual Review of Biophysics and Biomolecular Structure*, *30*, 129–155.

Palmer, A. G., Kroenke, C. D., & Loria, J. P. (2001). Nuclear magnetic resonance methods for quantifying microsecond-to-millisecond motions in biological macromolecules. *Methods in Enzymology*, *339*, 204–238.

Palmer, A. G., Wright, P. E., & Rance, M. (1991). Measurement of relaxation-time constants for methyl-groups by proton-detected heteronuclear NMR-spectroscopy. *Chemical Physics Letters*, *185*(1–2), 41–46.

Peng, J., Schwartz, D., Elias, J. E., Thoreen, C. C., Cheng, D., Marsischky, G., et al. (2003). A proteomics approach to understanding protein ubiquitination. *Nature Biotechnology*, *21*(8), 921–926.

Perrin, C. L., & Gipe, R. K. (1987). Rotation and solvation of ammonium ion. *Science*, *238*(4832), 1393–1394.

Peters, K. S., & Li, B. L. (1994). Picosecond dynamics of contact ion-pairs and solvent-separated ion-pairs in the photosolvolysis of diphenylmethyl chloride. *The Journal of Physical Chemistry*, *98*(2), 401–403.

Poon, D. K., Schubert, M., Au, J., Okon, M., Withers, S. G., & McIntosh, L. P. (2006). Unambiguous determination of the ionization state of a glycoside hydrolase active site lysine by 1H-15N heteronuclear correlation spectroscopy. *Journal of the American Chemical Society*, *128*(48), 15388–15389.

Radivojac, P., Vacic, V., Haynes, C., Cocklin, R. R., Mohan, A., Heyen, J. W., et al. (2010). Identification, analysis, and prediction of protein ubiquitination sites. *Proteins*, *78*(2), 365–380.

Sahu, D., Clore, G. M., & Iwahara, J. (2007). TROSY-based z-exchange spectroscopy: application to the determination of the activation energy for intermolecular protein translocation between specific sites on different DNA molecules. *Journal of the American Chemical Society*, *129*(43), 13232–13237.

Sarkar, S. K., Hiyama, Y., Niu, C. H., Young, P. E., Gerig, J. T., & Torchia, D. A. (1987). Molecular dynamics of collagen side chains in hard and soft tissues. A multinuclear magnetic resonance study. *Biochemistry*, *26*(21), 6793–6800.

Schanda, P., & Brutscher, B. (2005). Very fast two-dimensional NMR spectroscopy for real-time investigation of dynamic events in proteins on the time scale of seconds. *Journal of the American Chemical Society*, *127*(22), 8014–8015.

Schanda, P., Forge, V., & Brutscher, B. (2007). Protein folding and unfolding studied at atomic resolution by fast two-dimensional NMR spectroscopy. *Proceedings of the National Academy of Sciences of the United States of America*, *104*(27), 11257–11262.

Segawa, T., Kateb, F., Duma, L., Bodenhausen, G., & Pelupessy, P. (2008). Exchange rate constants of invisible protons in proteins determined by NMR spectroscopy. *ChemBioChem*, *9*(4), 537–542.

Simon, J. D., & Peters, K. S. (1982). Picosecond dynamics of ion-pairs—The effect of hydrogen-bonding on ion-pair intermediates. *Journal of the American Chemical Society*, *104*(24), 6542–6547.

Skelton, N. J., Palmer, A. G., Akke, M., Kordel, J., Rance, M., & Chazin, W. J. (1993). Practical aspects of 2-dimensional proton-detected N-15 spin relaxation measurements. *Journal of Magnetic Resonance Series B*, *102*(3), 253–264.

Skrynnikov, N. R., & Ernst, R. R. (1999). Detection of intermolecular chemical exchange through decorrelation of two-spin order. *Journal of Magnetic Resonance*, *137*(1), 276–280.

Szwarc, M. (1969). Ions and ion pairs. *Accounts of Chemical Research*, *2*(3), 87–96.

Takayama, Y., Castaneda, C. A., Chimenti, M., Garcia-Moreno, B., & Iwahara, J. (2008). Direct evidence for deprotonation of a lysine side chain buried in the hydrophobic core of a protein. *Journal of the American Chemical Society*, *130*(21), 6714–6715.

Tolman, J. R. (2001). Dipolar couplings as a probe of molecular dynamics and structure in solution. *Current Opinion in Structural Biology*, *11*(5), 532–539.

Tomlinson, J. H., Ullah, S., Hansen, P. E., & Williamson, M. P. (2009). Characterization of salt bridges to lysines in the protein G B1 domain. *Journal of the American Chemical Society*, *131*(13), 4674–4684.

Tugarinov, V., Hwang, P. M., Ollerenshaw, J. E., & Kay, L. E. (2003). Cross-correlated relaxation enhanced 1H[bond]13C NMR spectroscopy of methyl groups in very high molecular weight proteins and protein complexes. *Journal of the American Chemical Society*, *125*(34), 10420–10428.

Vijay-Kumar, S., Bugg, C. E., & Cook, W. J. (1987). Structure of ubiquitin refined at 1.8 A resolution. *Journal of Molecular Biology*, *194*(3), 531–544.

Voet, D., & Voet, J. G. (2004). *Biochemistry* (3rd ed.). Hoboken: Wiley.

Wang, Y. X., Jacob, J., Cordier, F., Wingfield, P., Stahl, S. J., Lee-Huang, S., et al. (1999). Measurement of 3hJNC′ connectivities across hydrogen bonds in a 30 kDa protein. *Journal of Biomolecular NMR*, *14*, 181–184.

Wei, A., Raymond, M. K., & Roberts, J. D. (1997). N-15 nuclear magnetic resonance spectroscopy. Changes in nuclear Overhauser effects and T-1 with viscosity. *Journal of the American Chemical Society*, *119*(12), 2915–2920.

Wennmohs, F., Staemmler, V., & Schindler, M. (2003). Theoretical investigation of weak hydrogen bonds to sulfur. *The Journal of Chemical Physics*, *119*(6), 3208–3218.

Yabe, T., & Kochi, J. K. (1992). Contact ion-pairs—Picosecond dynamics of solvent separation, internal return, and special salt effect. *Journal of the American Chemical Society*, *114*(12), 4491–4500.

Zandarashvili, L., Li, D. W., Wang, T., Brüschweiler, R., & Iwahara, J. (2011). Signature of mobile hydrogen bonding of lysine side chains from long-range ^{15}N-^{13}C scalar J-couplings and computation. *Journal of the American Chemical Society*, *133*(24), 9192–9195.